Gastroenterology 2020;159:2130–2145

S100A8 and S100A9 Are Important for Postnatal Development of Gut Microbiota and Immune System in Mice and Infants

Maike Willers,[1,*] **Thomas Ulas**,[2,3,*] Lena Völlger,[1] Thomas Vogl,[4] Anna S. Heinemann,[1] Sabine Pirr,[1] Julia Pagel,[5] Beate Fehlhaber,[1] Olga Halle,[6] Jennifer Schöning,[1] Sabine Schreek,[1] Ulrike Löber,[7] Morgan Essex,[7] Peter Hombach,[2] Simon Graspeuntner,[8] Marijana Basic,[9] Andre Bleich,[9] Katja Cloppenborg-Schmidt,[10] Sven Künzel,[11] Danny Jonigk,[12] Jan Rupp,[8] Gesine Hansen,[1,13] Reinhold Förster,[6,13] John F. Baines,[10,11] Christoph Härtel,[14,16] Joachim L. Schultze,[2,3] Sofia K. Forslund,[7,15] Johannes Roth,[4] and Dorothee Viemann[1,13,14]

[1]Department of Pediatric Pneumology, Allergology and Neonatology, Hannover Medical School, Hannover, Germany; [2]Genomics and Immunoregulation, LIMES-Institute, University of Bonn, Bonn, Germany; [3]PRECISE, Platform for Single Cell Genomics and Epigenomics at the German Center for Neurodegenerative Diseases and the University of Bonn, Bonn, Germany; [4]Institute of Immunology, University of Münster, Münster, Germany; [5]Department of Pediatrics, University of Lübeck, Lübeck, Germany; [6]Institute of Immunology, Hannover Medical School, Hannover, Germany; [7]Experimental and Clinical Research Center, a joint cooperation of Max-Delbrück Center for Molecular Medicine and Charité-Universitätsmedizin Berlin, Berlin, Germany; [8]Department of Infectious Diseases and Microbiology, University of Lübeck, Lübeck, Germany; [9]Institute for Laboratory Animal Science and Central Animal Facility, Hannover Medical School, Hannover, Germany; [10]Institute of Experimental Medicine, University of Kiel, Kiel, Germany; [11]Max Planck Institute for Evolutionary Biology, Plön, Germany; [12]Department of Pathology, Hannover Medical School, Hannover, Germany; [13]Cluster of Excellence RESIST (EXC 2155), Hannover Medical School, Hannover, Germany; [14]PRIMAL Consortium, Hannover Medical School, Hannover, Germany; [15]European Molecular Biology Laboratory, Structural and Computational Biology Unit, Heidelberg, Germany; and [16]Department of Pediatrics, University Hospital of Würzburg, Würzburg, Germany

BASIC AND TRANSLATIONAL AT

BACKGROUND & AIMS: After birth, the immune system matures via interactions with microbes in the gut. The S100 calcium binding proteins S100A8 and S100A9, and their extracellular complex form, S100A8–A9, are found in high amounts in human breast milk. We studied levels of S100A8–A9 in fecal samples (also called fecal calprotectin) from newborns and during infancy, and their effects on development of the intestinal microbiota and mucosal immune system. **METHODS:** We collected stool samples (n = 517) from full-term (n = 72) and preterm infants (n = 49) at different timepoints over the first year of life (days 1, 3, 10, 30, 90, 180, and 360). We measured levels of S100A8–A9 by enzyme-linked immunosorbent assay and analyzed fecal microbiomes by 16S sRNA gene sequencing. We also obtained small and large intestine biopsies from 8 adults and 10 newborn infants without inflammatory bowel diseases (controls) and 8 infants with necrotizing enterocolitis and measured levels of S100A8 by immunofluorescence microscopy. Children were followed for 2.5 years and anthropometric data and medical information on infections were collected. We performed studies with newborn C57BL/6J wild-type and *S100a9*$^{-/-}$ mice (which also lack S100A8). Some mice were fed or given intraperitoneal injections of S100A8 or subcutaneous injections of *Staphylococcus aureus*. Blood and intestine, mesenterial and celiac lymph nodes were collected; cells and cytokines were measured by flow cytometry and studied in cell culture assays. Colon contents from mice were analyzed by culture-based microbiology assays. **RESULTS:** Loss of S100A8 and S100A9 in mice altered the phenotypes of colonic lamina propria macrophages, compared with wild-type mice. Intestinal tissues from neonatal S100-knockout mice had reduced levels of CX3CR1 protein, and *Il10* and *Tgfb1* mRNAs, compared with wild-type mice, and fewer T-regulatory cells. S100-knockout mice weighed 21% more than wild-type mice at age 8 weeks and a higher proportion developed fatal sepsis during the neonatal period. S100-knockout mice had alterations in their fecal microbiomes, with higher abundance of Enterobacteriaceae. Feeding mice S100 at birth prevented the expansion of Enterobacteriaceae, increased numbers of T-regulatory cells and levels of CX3CR1 protein and *Il10* mRNA in intestine tissues, and reduced body weight and death from neonatal sepsis. Fecal samples from term infants, but not preterm infants, had significantly higher levels of S100A8–A9 during the first 3 months of life than fecal samples from adults; levels decreased to adult levels after weaning. Fecal samples from infants born by cesarean delivery had lower levels of S100A8–A9 than from infants born by vaginal delivery. S100 proteins were expressed by lamina propria macrophages in intestinal tissues from infants, at higher levels than in intestinal tissues from adults. High fecal levels of S100 proteins, from 30 days to 1 year of age, were associated with higher abundance of Actinobacteria and Bifidobacteriaceae, and lower abundance of Gammaproteobacteria—particularly opportunistic Enterobacteriaceae. A low level of S100 proteins in infants' fecal samples associated with development of sepsis and obesity by age 2 years. **CONCLUSION:** S100A8 and S100A9 regulate development of the intestinal microbiota and immune system in neonates. Nutritional supplementation with these proteins might aide in development of preterm infants and prevent microbiota-associated disorders in later years.

Keywords: BMI; Gut Mucosal Immunity; NEC; Treg Cells.

Colonizing microbes provide the newborn immune system with crucial instructing information that induces postnatal maturation of immunity.[1,2] This co-development ideally results in a balanced homeostasis between the host and the microbiota,[3] whereas alterations predispose individuals to inflammatory and metabolic diseases.[4–7] Specific microbiota compositions have been described to precede necrotizing enterocolitis (NEC)[8] in preterm infants and to be important direct sources of sepsis-causing bacterial translocation.[9,10] Except for full-term birth, vaginal delivery (VD), and breastfeeding,[11–16] little is known about what host factors influence the interplay between intestinal immunity and initial gut colonization to ensure developing homeostasis.

In healthy neonates, high serum concentrations of the endogenous Toll-like receptor 4 ligands S100A8 and S100A9 induce a state of microbial hyporesponsiveness in blood monocytes, also described as "stress tolerance."[17–19] Physiologically, they form a heterodimer complex (S100A8-A9) known as calprotectin.[20,21] Later in life, when acutely released during inflammatory settings, S100A8-A9 exerts primarily amplifying effects and serves as biomarker of inflammation, for example, fecal calprotectin (hereafter "fS100A8-A9") in inflammatory bowel disease (IBD).[22] Breast milk contains extremely high levels of S100A8-A9[23] and fS100A8-A9 levels are high in healthy breast-fed infants.[24] After birth, blood-derived (BD) monocytes replace yolk sac–derived intestinal macrophages and differentiate into tissue-resident lamina propria macrophages (LPMPs).[25–27] The invasion of S100-primed neonatal monocytes together with the high local supply at the luminal site via breast milk prompted us to speculate about S100A8-A9 playing an important role for the postnatal development of intestinal immunity and microbial colonization.

We found that high levels of fS100A8-A9 in the neonatal gut induce a regulatory LPMP phenotype permissive for the expansion of regulatory T cells (Tregs), which promotes a favorable development of the gut microbiota. The clinical relevance is corroborated by strong associations of neonatal fS100A8-A9 deficiency with dysbiosis-linked diseases like NEC, sepsis, and obesity, which can experimentally be prevented by a single nutritional supply of S100A8 at birth.

WHAT YOU NEED TO KNOW

BACKGROUND AND CONTEXT

After birth, the immune system develops via interactions with microbes in the gut. S100A8 and S100A9 (also called calprotectin) are immune-stimulatory S100 calcium binding proteins present in high amounts in breast milk.

NEW FINDINGS

S100A8 and S100A9 regulate development of the intestinal microbiota and immune system in neonates.

LIMITATIONS

Further studies are needed to determine the effects of S100 proteins in humans and in newborns.

IMPACT

Nutritional supplementation with S100 proteins might aide in development of preterm infants and prevent microbiota-associated disorders during childhood.

Materials and Methods

Human Samples

Stool samples were collected from 2 birth cohorts of healthy term (n = 72, Supplementary Table 1) and preterm (n = 49, 23 to 32 gestational weeks, Supplementary Table 2) infants prospectively enrolled at the Hannover Medical School respective the University Hospital of Lübeck. Late-onset sepsis (LOS) was defined as sepsis starting after 72 hours of life. Biopsies of human small intestine (SI) and large intestine (LI) were obtained from n = 8 adults and n = 10 newborn infants without underlying IBD (controls) and n = 8 patients with NEC (Supplementary Table 3). Written informed consent was obtained from all parents and donors. For details see Supplementary Experimental Procedures.

Mice and Mouse Studies

Mouse strains housed under specific pathogen-free conditions were the Foxp3-eGFP reporter mouse B6.Cg-Foxp3 tm1 Mal/J for the isolation of naïve $CD4^+$ T cells, and the C57BL/6J wild-type (WT) mouse and the *S100a9*$^{-/-}$ mouse[28] (also deficient for S100A8 due to the dependency of the post-transcriptional stability of S100A8 on the presence of S100A9[28,29] and the failure to form heterocomplexes[20,21]) to harvest colons and mesenterial and celiac lymph nodes. In indicated experiments, *S100a9*$^{-/-}$ pups were injected intraperitoneally (IP) or fed per os within 24 hours after birth with recombinant murine S100A8 or phosphate-buffered saline (controls). For details regarding mating and cross-fostering settings, cell isolation, immunofluorescence microscopy of tissue samples, and of murine fecal samples, see Supplementary Experimental Procedures.

Murine Model of Neonatal Sepsis

At the age of 3 days, mice were infected subcutaneously with 7×10^4 colony-forming units (CFU) of *Staphylococcus aureus* and returned to their mothers. Mice were monitored over 80 hours for survival or killed 24 hours after infection to harvest blood for cytokine measurements and organs. Bacterial

* Authors share co-first authorship.

Abbreviations used in this paper: **BD, blood-derived; BMI, body mass index; CS, cesarean section; CX3CR1, chemokine (C-X3-C motif) receptor 1; IL-1β, interleukin-1 beta; IP, intraperitoneally; LI, large intestine; LOS, late-onset sepsis; LPMP, lamina propria; LPS, lipopolysaccharide; MOD, mode of delivery; NEC, necrotizing enterocolitis; SI, small intestine; TGF-β, transforming growth factor beta; TNF-α, tumor necrosis factor-alpha; Treg, T-regulatory cell; VD, vaginal delivery; WT, wild-type; YS, yolk sac.**

Most current article

0016-5085
https://doi.org/10.1053/j.gastro.2020.08.019

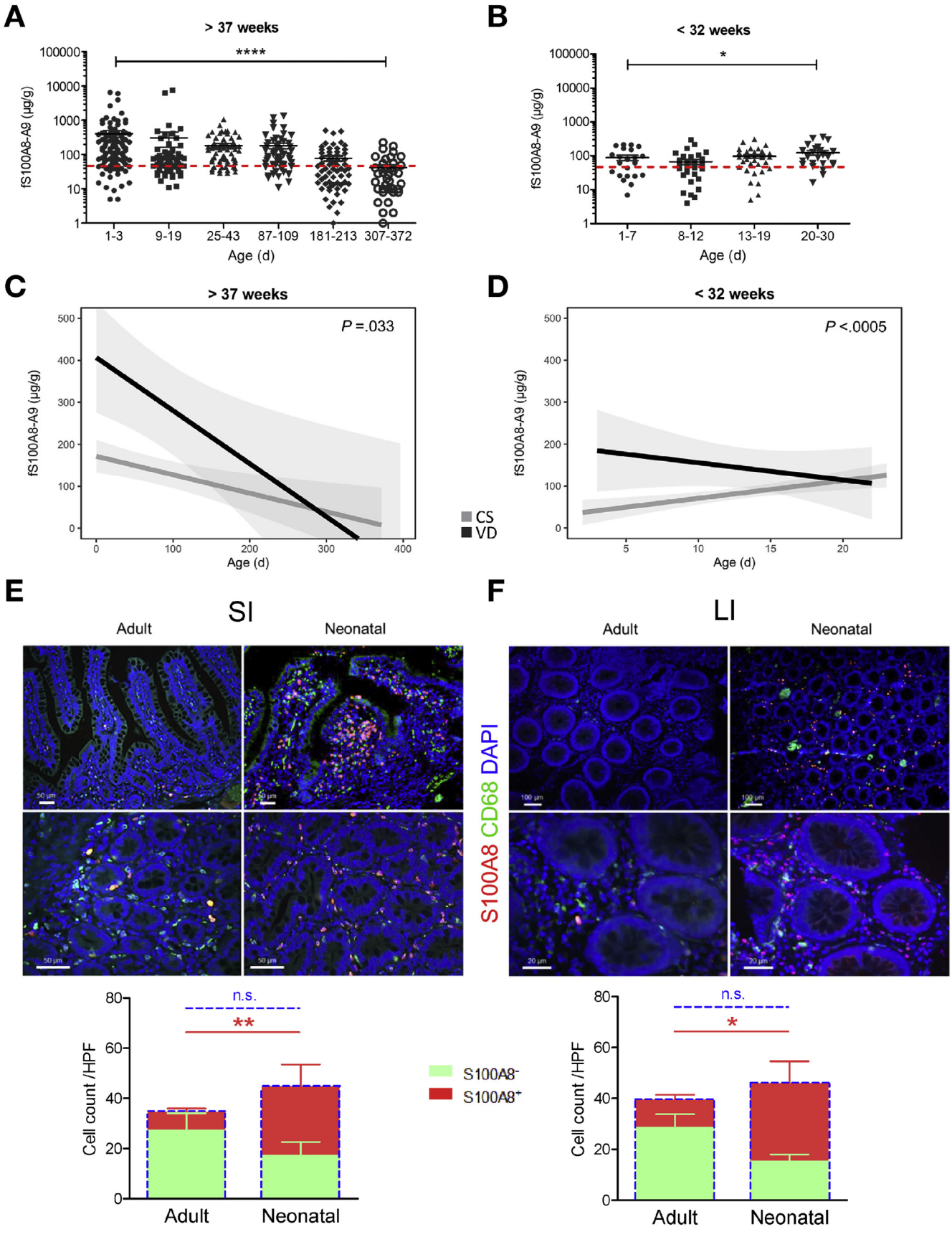
A
> 37 weeks
****
fS100A8-A9 (µg/g)
100000
10000
1000
100
10
1
1-3
9-19
25-43
87-109
181-213
307-372
Age (d)
B
< 32 weeks
*
fS100A8-A9 (µg/g)
1-7
8-12
13-19
20-30
Age (d)
C
> 37 weeks
P =.033
fS100A8-A9 (µg/g)
Age (d)
D
< 32 weeks
P <.0005
fS100A8-A9 (µg/g)
Age (d)
CS
VD
E
SI
Adult
Neonatal
F
LI
Adult
Neonatal
S100A8 CD68 DAPI
n.s.
**
Cell count /HPF
S100A8-
S100A8+
Adult
Neonatal
n.s.
*
Cell count /HPF
Adult
Neonatal

burden was determined as described previously[17] by plating homogenates of lungs and livers onto blood-agar plates and counting bacterial colonies after 18 hours of incubation at 37°C.

Cell Culture Assays

LPMPs were ex vivo incubated with lipopolysaccharide (LPS) or phosphate-buffered saline and processed for gene expression studies. LPMPs were co-cultured with naïve T cells from Foxp3-eGFP reporter mice to assess their Treg-inducing capacity. For details of cell culture conditions, flow cytometry and quantitative reverse transcriptase polymerase chain reaction, see Supplementary Experimental Procedures.

16S rRNA Gene Bacterial Profiling

16S rRNA gene profiling of human fecal samples was performed as described previously.[10] DNA was isolated using the PowerSoil DNA Isolation Kit (MOBIO, Carlsbad, Canada) with an additional 1.5-hour Protease K incubation before the first centrifugation step. From each DNA sample, the V3-V4 region of the 16S rRNA gene was amplified using primers spanning the V3-V4 hypervariable regions (Supplementary Table 4). PCR including quantification of amplicons and library preparation was performed as described elsewhere.[30] Equimolar amounts of the correct-sized amplicons were pooled for sequencing. Sequencing including negative extraction controls was performed on an Illumina MiSeq sequencer using the MiSeq Reagent Kit v3 (600 cycles) (Illumina, San Diego, CA). For details of bioinformatics of 16S rRNA gene sequencing data and nested model comparisons, see Supplementary Experimental Procedures.

Cytokine Studies

Plasma levels of tumor necrosis factor-alpha (TNF-α) and interleukin-1 beta (IL-1β) were measured by using murine LEGENDplex assays (BioLegend, San Diego, CA). FACS Canto II flow cytometer was used for measurements and LEGENDplex Data Analysis Software v7.0 (BioLegend) for data analysis.

Statistical Analysis

Statistically significant *P* values are indicated by asterisks. Tests are specified in figure legends. For details of statistical tests, see Supplementary Experimental Procedures.

Data Availability

16S rRNA sequencing files were submitted to the National Center for Biotechnology Information Sequence Read Archive (www.ncbi.nlm.nih.gov/sra) and are available with BioProject accession number PRJNA514340.

Results

Abundant S100A8-A9 in the Gut of Healthy Infants

To obtain a comprehensive picture of fS100A8-A9 levels in newborn infants, 517 stool samples collected from a birth cohort of 72 healthy term infants (Supplementary Table 1) and 49 preterm infants (Supplementary Table 2) were analyzed. In term infants, fS100A8-A9 levels are significantly higher during the first 3 months of life compared with normal adult values and normalize along with weaning until the end of the first year (Figure 1*A*). In preterm infants, initial fS100A8-A9 levels are significantly lower than in term infants (Supplementary Figure 1*A*), but increase during the first month of life (Figure 1*B*). In both cohorts, fS100A8-A9 levels were dependent on the mode of delivery (MOD) with higher levels after VD than cesarean section (CS) (Figure 1*C* and *D*), particularly after primary CS (Supplementary Figure 1*B*). In term infants, the MOD impacts on fS100A8-A9 levels only in the first week of life, but in preterm infants until the third week of life (Supplementary Figure 1*C* and *D*). Breast milk is one important source of fS100A8-A9 in newborn infants.[23,24] To investigate whether S100A8-A9 is also produced endogenously in the neonatal gut, we used human SI and LI tissue samples of newborn and adult patients without underlying IBD. Under these physiologic conditions, S100-protein expression is detectable in LPMPs but not in intestinal epithelial cells, with the proportion of S100A8-expressing LPMPs being significantly higher in the SI (Figure 1*E*) and LI (Figure 1*F*) of neonates compared with adults. Thus, the gut of healthy neonates is exposed to high amounts of S100A8-A9, while deficient states are particularly observed in preterm infants delivered by CS.

High fS100A8-A9 During Infancy Supports Developing Gut Eubiosis

To assess whether physiologically high fS100A8-A9 in neonates plays a role for the development of the gut microbiome we generated 16S rRNA gene profiles of 414 stool samples from the term infant cohort. Overall diversity of gut microbiota composition significantly increases during the first year of life (Figure 2*A*) and follows known

Figure 1. Postnatal abundance of S100A8-A9 in the human intestinal tract. (*A–D*) S100A8-A9 levels in fecal samples collected at indicated ages from a cohort of (*A,C*) healthy term infants (n = 72) and (*B, D*) preterm infants (n = 48). (*A, B*) *Bars* on a logarithmic scale represent means ± SEM. *$P < .05$, ****$P < .0001$ (Kruskal-Wallis test). *Dotted line* indicates the cutoff for normal adult fS100A8-A9 levels (50 μg/g). (*C, D*) Regression of fS100A8-A9 levels subgrouped according to the MOD (*gray-shaded* 95% confidence interval). *P* value indicates differences between both groups (likelihood ratio tests of nested models with/without MOD as predictor beyond age). (*E, F*) *Top*, representative images of human adult and neonatal SI (*E*) and LI (*F*) tissue samples from individuals without underlying intestinal inflammation immunostained for S100A8 (*red*), CD68 (*green*), and nuclei (with 4′,6-diamidino-2-phenylindole [DAPI]; *blue*). Bottom, total number of $CD68^+$ LPMPs (*blue dotted bar*) differentiated in $S100A8^-CD68^+$ LPMPs (*green bar* section) and $S100A8^+CD68^+$ LPMPs (*red bar* section). Values represent means ± SEM of counts in 4 high-power fields of n = 4 adult and n = 6 neonatal SI samples (*E*) and n = 4 adult and n = 4 neonatal LI samples (*F*). *$P < .05$, **$P < .005$ (Mann-Whitney *U* test).

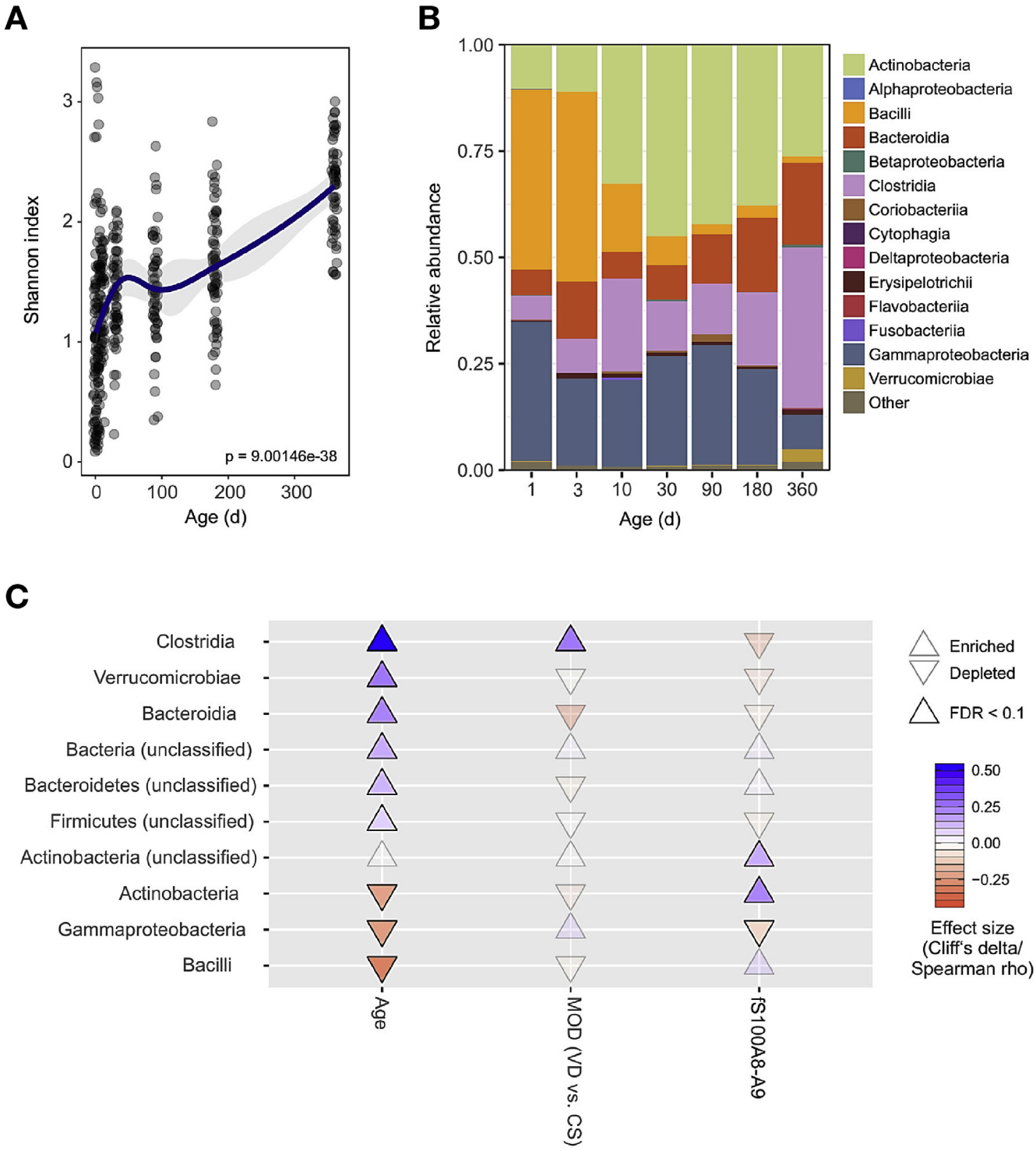

Figure 2. High fS100A8-A9 levels are associated with an eubiotic infant gut state. (*A–C*) 16S ribosomal RNA (rRNA) gene sequencing data determined in 414 stool samples collected from 72 human term infants (day 1: n = 57, day 3: n = 51, day 10: n = 66, day 30: n = 63, day 90: n = 59, day 180: n = 62, day 360: n = 56). (*A*) Shannon index of individual 16S rRNA profiles and linear regression line (*gray-shaded* 95% confidence interval) across the first year of life. Significance (*P*) of changes over time (general mixed regression model treating subject as a random effect for stratification, analysis of variance F-test). (*B*) Mean relative abundance of bacterial taxa at class level. (*C*) Cuneiform plot (marker direction and hue shows effect direction, marker intensity effect size) of gut bacterial taxa at class level significantly (Spearman or Mann-Whitney *U* false discovery rate [FDR] <0.1, nested model test FDR <0.1) and strongly (absolute Spearman rho or Cliff's delta effect size >0.2) impacted by age, MOD, or fS100A8-A9 across infancy (≥30 days to 1 year), when adjusting (nested mixed effects model comparison) for each of the other 2 variables. *Bold markers* fulfill significance criteria, *gray-edged markers* do not and are shown for comparison only.

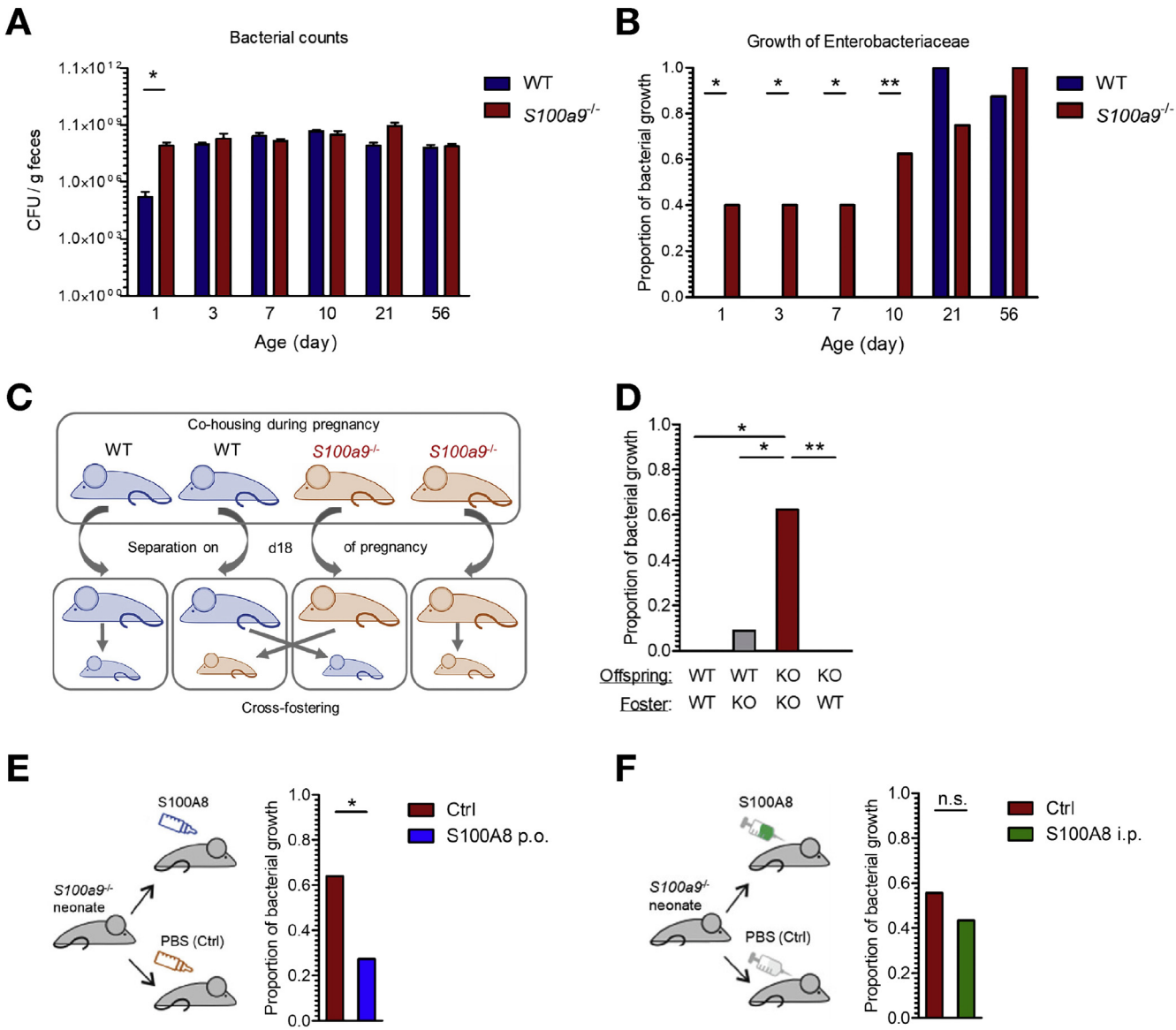

Figure 3. Enterally supplied immunoregulatory S100-alarmins and the gut microbiota. (A,B) Fecal samples collected from the WT and S100a9–/– offspring at indicated ages (each n = 10–13). (A) Total bacterial counts cultured in aerobic conditions. CFU, colony-forming units. *P < .05 (unpaired t-test). (B) Proportion of mice with Enterobacteriaceae-positive feces (each n = 8–13). (C, D) The offspring of WT and S100a9–/– (KO) mothers was co-fostered and cross-fostered. (C) Experimental setup. (D) Proportion of mice with Enterobacteriaceae-positive feces at day 10 (each n = 8–11). (E,F) Proportion of S100a9–/– mice with Enterobacteriaceae-positive feces at day 10 after (E) feeding or (F) IP injection of S100A8 or phosphate-buffered saline (PBS) (Ctrl) within 24 hours after birth (each n = 22–25). *P <.01, **P <.005, n.s., not significant (sign tests).

dynamics in bacterial classes,[2,11,16] most prominent the increase of Actinobacteria, Bacteroidia, and Clostridia and the decrease of Bacilli and Gammaproteobacteria (Figure 2*B*). To test the impact of fS100A8-A9 and MOD on longitudinal microbiome features nested model comparisons were performed using strict filter criteria for differential taxon abundances while accounting for confounding influences. The initial colonization pattern (birth to 10 days), especially that of Bacilli, Bacteroidia, Clostridia, and Gammaproteobacteria, is primarily determined by the MOD but not fS100A8-A9 (Supplementary Figure 2 and Supplementary Table 5). However, after that period, MOD impact only remains detectable for the expansion of Clostridia. In contrast, high fS100A8-A9 levels during entire infancy (≥30 days to 1 year) are linked to a specific microbiome signature correlating with a higher abundance of Actinobacteria and anti-correlating with the abundance of Gammaproteobacteria (Figure 2*C* and Supplementary Table 5). At the family level, fS100A8-A9 has particular impact on the expansion of Bifidobacteriaceae, and in turn contributes to the reduction of Enterobacteriaceae in the infant's gut (Supplementary Table 5). Prediction models based on these gut microbial communities revealed significant effects on the abundance gut metabolic pathways of fS100A8-A9 after the first 10 days of life, but not of the MOD (Supplementary Table 5), with fS100A8-A9 promoting production and inhibiting

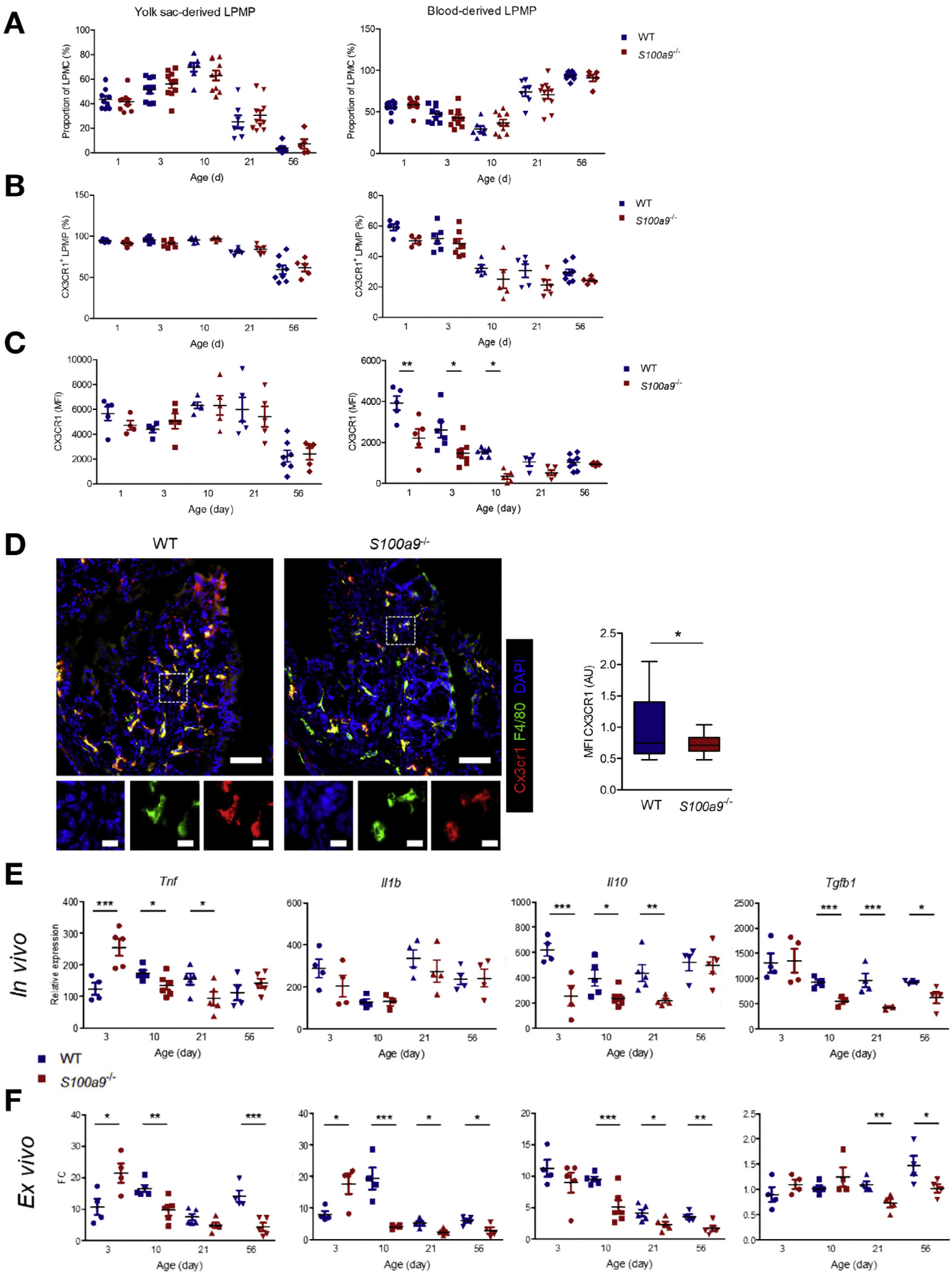
A
Yolk sac-derived LPMP
Blood-derived LPMP
Proportion of LPMC (%)
Age (d)
WT
S100a9-/-
B
CX3CR1+ LPMP (%)
C
CX3CR1 (MFI)
Age (day)
D
WT
S100a9-/-
Cx3cr1 F4/80 DAPI
MFI CX3CR1 (AU)
E
In vivo
Tnf
Il1b
Il10
Tgfb1
Relative expression
F
Ex vivo
FC

degradation of short-chain fatty acids (Supplementary Figure 3). The data suggest that S100-alarmins are crucial for promoting a favorable infant gut state of abundant Actinobacteria-like Bifidobacteriaceae and growth restriction of Gammaproteobacteria including pathobiont Enterobacteriaceae, resulting in a shift toward health-promoting gut metabolic functions.

To get further mechanistic insight, we performed mouse experiments using WT and *S100a9*$^{-/-}$ mice. Dams were co-housed to ensure comparability of the mother's gut microbiota and separated on day 18 of pregnancy shortly before giving birth. In the WT and *S100a9*$^{-/-}$ offspring, no striking difference is detectable in the overall fecal bacterial count (Figure 3*A*). However, while cultivable amounts of Enterobacteriaceae, mainly *Escherichia coli* based on its characteristic morphology on MacConkey agar, in the *S100a9*$^{-/-}$ offspring are already detectable from day 1 on, they are not observed in WT mice before weaning (day 21) (Figure 3*B*).

In a cross-fostering setting, early-life overgrowth of Enterobacteriaceae is completely abrogated in *S100a9*$^{-/-}$ neonates fostered by WT mothers, while in WT neonates fostered by *S100a9*$^{-/-}$ mothers, cultivable amounts of Enterobacteriaceae get traceable already on day 10 (Figure 3*C* and *D*). Thus, endogenous production of S100A8-A9 alone is insufficient in order to achieve full effect, which instead requires supplementation by S100-alarmins via breast milk, whereas the effect of breast milk-derived S100A8-A9 alone is full restriction of Enterobacteriaceae growth.

To exclude direct antimicrobial effects from S100-alarmins by chelating Mn^{2+} and Zn^{2+},[23,31,32] we supplied *S100a9*$^{-/-}$ neonates with the S100A8 homodimer that lacks binding sites for divalent metal ions.[21,32,33] A one-time feeding of S100A8 after birth is sufficient to successfully limit the subsequent expansion of Enterobacteriaceae (Figure 3*E*) suggesting that the S100-priming of neonatal intestinal immunity is important for the microbiota-shaping effect, whereas the systemic administration of S100A8 at a dose strongly immunoregulatory for blood monocytes[17,18] has no significant impact on the abundance of Enterobacteriaceae (Figure 3*F*).

Collectively, our findings clearly reveal that high fS100A8-A9 in infants affects the mutual relationship between the host and the gut microbiota in a beneficial manner by restricting the growth of pathobiont Gammaproteobacteria, particularly Enterobacteriaceae including *E coli*, and promoting the colonization with eubiont Actinobacteria including Bifidobacteriaceae.

S100-alarmins Regulate LPMPs

To explore how S100A8-A9 primes intestinal immunity, we isolated colonic LPMPs from WT and *S100a9*$^{-/-}$ mice at day defined ages (Supplementary Figure 4*A* and *B*). Morphologically, there are no differences between WT and *S100a9*$^{-/-}$ LPMPs (Supplementary Figure 4*C*) or numeric alterations in the proportions or the replacement of yolk sac LPMPs by BD-LPMPs[27] (Figure 4*A* and Supplementary Figure 4*B*). The same holds true for the proportion of chemokine (C-X3-C motif) receptor 1 (CX3CR1)-positive LPMPs (Figure 4*B*). However, the mean expression of CX3CR1 is significantly lower on *S100a9*$^{-/-}$ BD-LPMPs compared with WT BD-LPMPs during the neonatal period and adolescence (Figure 4*C* and *D*). Next, freshly isolated LPMPs were used to capture the in vivo tuned baseline of gene expression (Figure 4*E*). In *S100a9*$^{-/-}$ LPMPs, *Tnf* is significantly higher expressed on day 3, but lower on day 10 and day 21 than in WT LPMPs, whereas the expression of *Il1b* is comparable. The microbial responsiveness of the LPMPs was studied by ex vivo LPS stimulation (Figure 4*F*). On day 3, *S100a9*$^{-/-}$ LPMPs respond with a significantly stronger expression of *Tnf* and *Il1b*, whereas from day 10 the pattern switches to a significantly reduced inducibility of these proinflammatory genes compared with WT LPMPs. During the first postnatal days, the extreme high levels of S100A8-A9 apparently tolerize the LPS response of LPMPs, whereas with increasing age while basal S100A8-A9 levels decrease its amplifier function takes effect on induction.[19,34–36] In contrast, the regulatory genes *Il10* and transforming growth factor-β (*Tgfb1*) show nearly constant basal (Figure 4*E*) as well as LPS-induced (Figure 4*F*) expression deficits in *S100a9*$^{-/-}$ LPMPs compared with WT LPMPs, pointing to an important impact of S100A8-A9 on the regulatory phenotype of LPMPs.

S100-primed LPMPs Promote the Expansion of Tregs

CX3CR1, IL-10, and TGF-β have been identified as important triggers for the expansion of Tregs.[37–40] We therefore performed age-dependent analyses (Supplementary Figure 5*A* and *B*) revealing that the initial influx of Tregs into the colonic lamina propria and their proportion in mesenterial lymph nodes and celiac lymph

Figure 4. Differential programming of WT and *S100a9*$^{-/-}$ LPMPs. (*A–C*) LPMCs isolated from the LI of WT and *S100a9*$^{-/-}$ mice were analyzed by flow cytometry. (*A*) Proportion of yolk sac (YS)-LPMPs and BD-LPMPs. (*B*) Percent CX3CR1^{+} YS-LPMPs and BD-LPMPs. (*C*) CX3CR1 level on YS-LPMPs and BD-LPMPs. *Bars* represent means ± SEM. **P* <.05, ***P* <.01, ****P* <.005 (post hoc unpaired *t*-test) (each n = 4–11). MFI, mean fluorescence intensity. (*D*) *Upper left panels*, representative images of LI tissue samples from day 10 WT and *S100a9*$^{-/-}$ mice immunostained for CX3CR1 (*red*), F4/80 (*green*), and nuclei (DAPI; *blue*). Scale bar, 50 μm. *Lower left panels*, single color stainings of the dotted zoom-out. Scale bars, 10 μm. *Right*, CX3CR1 expression by F4/80^{+} LPMPs. Box plots show medians, interquartile ranges and total ranges of the MFI of CX3CR1 per F4/80^{+} region of interest (ROI) determined in 14 randomly selected images. **P* < .01 (unpaired *t*-test). (*E, F*) Expression of indicated genes in LPMPs isolated from the LI of WT and *S100a9*$^{-/-}$ mice at indicated ages. (*E*) Basal expression level (in vivo) and (*F*) ex vivo LPS-induced fold changes of expression. Plots represent means ± SEM (each n = 3–6). **P* < .05, ***P* < .01, ****P* < .005 (post hoc unpaired *t*-test).

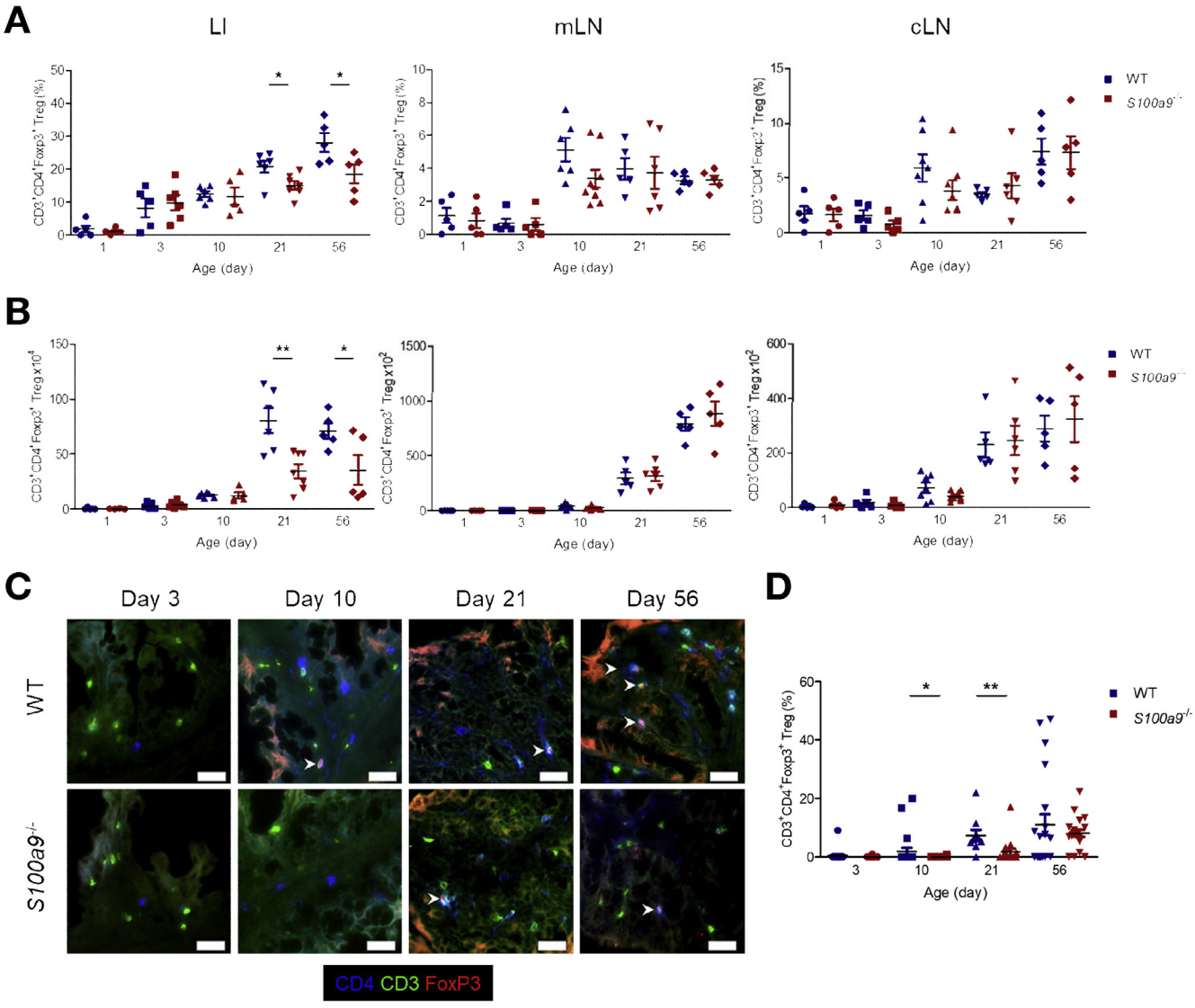
A
LI
mLN
cLN
WT
S100a9-/-
Age (day)
B
C
Day 3
Day 10
Day 21
Day 56
WT
S100a9-/-
CD4 CD3 FoxP3
D
E
Foxp3/EGFP naive T cells
WT or S100a9-/- LPMPs
anti-CD3/CD28
IL-2
± TGF-β
± IL-10
FACS: Proportion of Tregs
F
w/o TGF-β + IL-10
T cell : LPMP ratio
10:1
5:1
G
TGF-β
H
TGF-β + IL-10
n.s.
T cells only
WT LPMPs
S100a9-/- LPMPs

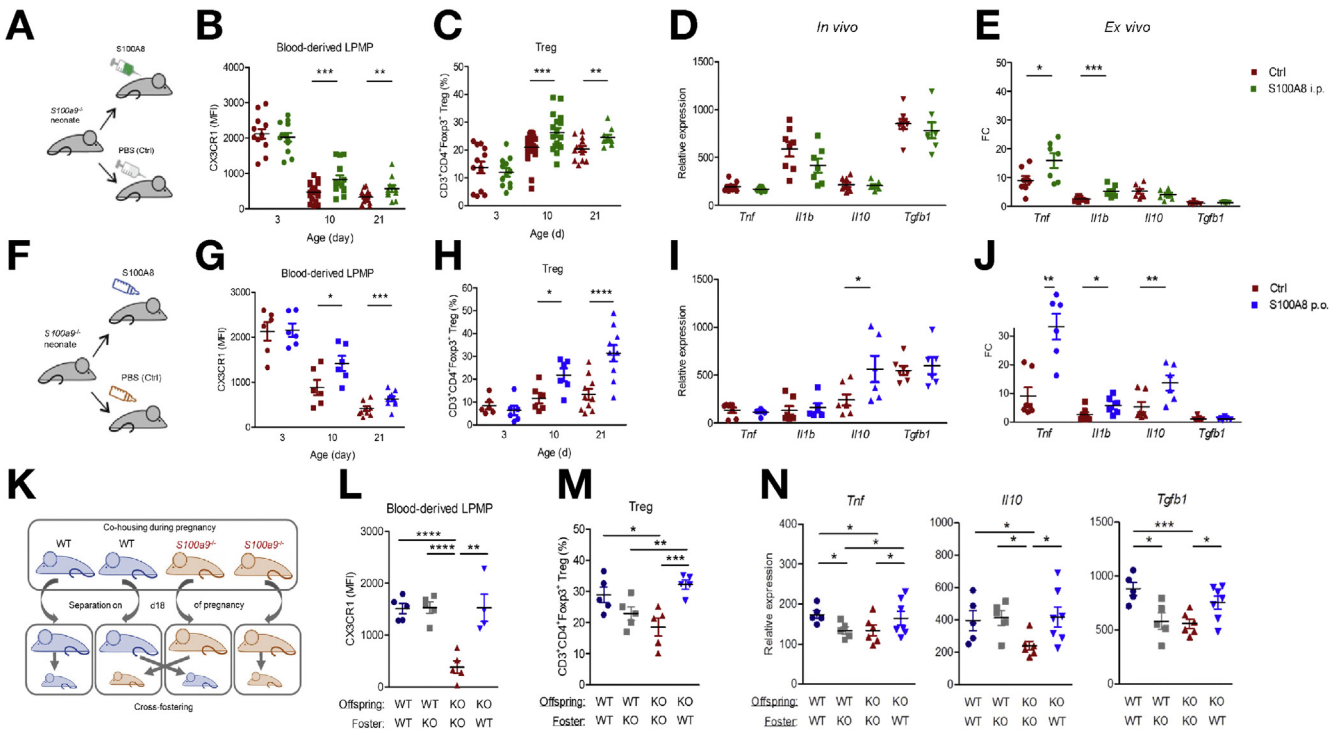

Figure 6. S100-priming of the neonatal gut modulates the development of mucosal immunity. (A–J) LPMCs from S100a9–/– neonates supplemented within the first 24 hours after birth with S100A8 or phosphate-buffered saline (PBS) (controls, Ctrl) via the (A-E) IP route or (F–J) enteral (per os) route. (B, G) CX3CR1 (mean fluorescence intensity [MFI]) on BD-LPMPs (each n = 11–18) and (C, H) fractions of CD3+CD4+FoxP3+ Tregs in CD3+ T cells (each n = 6–10). (D, I) Relative basal expression (in vivo) and (E, J) ex vivo LPS-induced fold changes of expression of indicated genes in day 10 LPMPs from S100a9–/– neonates supplemented after birth IP (D, E, each n = 7–8) or per os (I, J, each n = 6–7) with S100A8 or PBS (Ctrl). (K–N) The offspring of WT and S100a9–/– mothers were co-fostered and cross-fostered (each group n = 4–7). (K) Experimental setup. (L) CX3CR1 (MFI) on BD-LPMPs, (M) proportions of CD3+CD4+FoxP3+ Tregs in CD3+ T cells and (N) relative basal expression of indicated genes in day 10 LPMPs. Plotted are means ± SEM. *P < .05, **P < .01, ***P < .005, ****P < .0005 (post hoc unpaired t-test).

nodes are comparable in WT and *S100a9*$^{-/-}$ mice. However, the subsequent expansion of Tregs in the colon is significantly impaired in adolescent *S100a9*$^{-/-}$ mice compared with WT mice (Figure 5*A–D*). In co-culture, Tregs are significantly better inducible from naïve T cells in the presence of WT LPMPs than *S100a9*$^{-/-}$ LPMPs (Figure 5*E* and *F*). Supplementation of TGF-β increases the overall yield of Tregs that nevertheless still remains lower in co-culture with *S100a9*$^{-/-}$ LPMPs compared with WT LPMPs (Figure 5*G*). The additional supplementation of IL-10, however, compensates for the deficient Treg-inducing capacity of *S100a9*$^{-/-}$ LPMPs (Figure 3*H*). These findings suggest that the S100A8-A9–induced LPMP phenotype promotes the postnatal development of Tregs in the colonic mucosa particularly by providing IL-10.

Imprinting of Neonatal Gut Immunity by S100-alarmins

S100A8 homodimers are the most immunoactive form of S100-alarmins.[17–20] We tested the immunomodulatory potential of a single IP injection or a one-time feeding of S100A8 within 24h after birth on gut immunity in *S100a9*$^{-/-}$ pups (Figure 6*A* and *F*). From day 10 on, we observed

Figure 5. *S100a9*$^{-/-}$ LPMPs do not support the expansion of Tregs. (*A*) Proportion of CD3$^+$CD4$^+$FoxP3$^+$ Tregs in CD3$^+$ T cells and (*B*) absolute Treg numbers in the lamina propria of the LI, mesenteric lymph nodes (mLN) and celiac lymph nodes (cLN) harvested from WT and *S100a9*$^{-/-}$ mice. Plots represent means ± SEM (each n = 5–8). *$P < .05$, **$P < .01$ (post hoc unpaired *t*-test). (*C, D*) Immunofluorescence microscopy of Tregs in LI tissue samples from WT and *S100a9*$^{-/-}$ mice aged 3, 10, 21, and 56 days. (*C*) Representative images, immunostained for CD4 (*blue*), CD3 (*green*), and FoxP3 (*red*). Scale bar, 50 μm. *Arrowheads* mark CD3$^+$CD4$^+$FoxP3$^+$ Tregs. (*D*) Means ± SEM of the fraction of CD3$^+$CD4$^+$FoxP3$^+$ Tregs in CD3$^+$ T cells. *$P < .05$, **$P < .005$ (post hoc unpaired *t*-test). (*E–H*) Naïve T cells isolated from spleens of Foxp3-eGFP reporter mice were cultured for 4 days alone or with colonic WT or *S100a9*$^{-/-}$ LPMPs in the presence of anti-CD3/CD28 and IL-2. (*E*) Experimental setup. (*F*) Proportions of induced Tregs at T cell:LPMP ratios of 10:1 and 5:1. (*G, H*) Proportions of induced Tregs with additional presence of TGF-β (*G*) or TGF-β and IL-10 (*H*) (T cell:LPMP ratios 5:1). *Bars* represent means ± SEM (each group n = 3–5) *$P < .05$, **$P < .01$, ***$P < .001$ (post hoc analysis of variance *t*-tests).

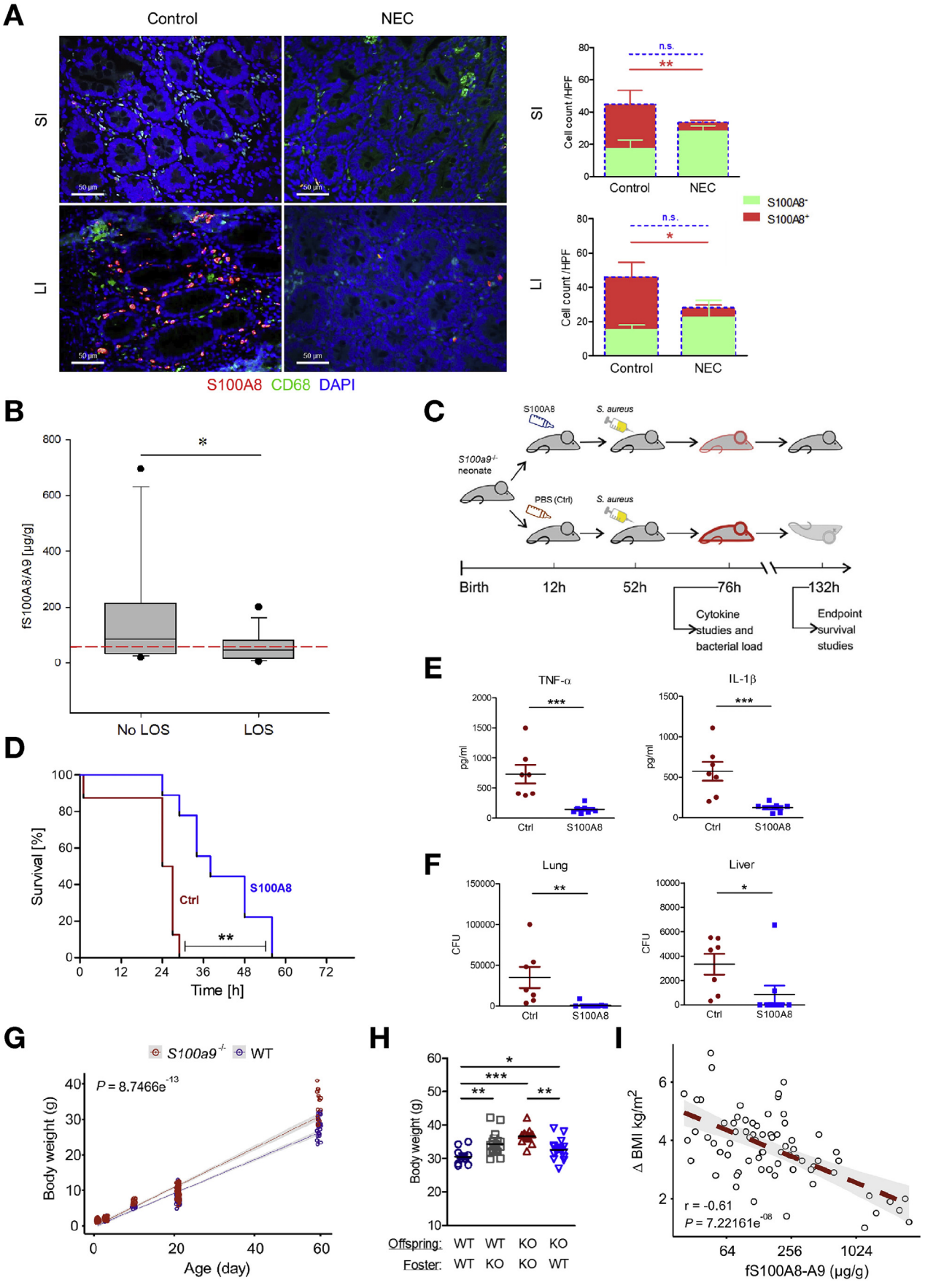
A
Control
NEC
SI
LI
50 µm
S100A8 CD68 DAPI
Cell count /HPF
n.s.
**
*
Control
NEC
S100A8-
S100A8+
B
fS100A8/A9 [µg/g]
*
No LOS
LOS
C
S100A8
S. aureus
S100a9-/- neonate
PBS (Ctrl)
Birth
12h
52h
76h
132h
Cytokine studies and bacterial load
Endpoint survival studies
D
Survival [%]
Ctrl
S100A8
**
Time [h]
E
TNF-α
IL-1β
pg/ml
***
Ctrl
S100A8
F
Lung
Liver
CFU
**
*
G
S100a9-/-
WT
P = 8.7466e-13
Body weight (g)
Age (day)
H
Body weight (g)
Offspring: WT WT KO KO
Foster: WT KO KO WT
I
Δ BMI kg/m2
r = -0.61
P = 7.22161e-08
fS100A8-A9 (µg/g)

significantly higher level of CX3CR1 on LPMPs after S100A8 supplementation compared with control mice, independent of the route of administration (Figure 6*B* and *G*). Likewise, Tregs expand significantly better after S100A8 application, particularly via the enteral route (Figure 6*C* and *H*). S100A8 effects on the transcriptional programming were assessed on day 10 when the baseline expression of *Il10* and *Tgfb1* and the LPS-inducibility of *Tnf*, *Il1b*, and *Il10* are impaired in *S100a9*$^{-/-}$ LPMPs (Figure 4*E* and *F*). S100A8 given IP has no effect on the basal expression of *Il10* and *Tgfb1* (Figure 6*D*) and only improves the LPS-inducibility of *Tnf* and *Il1b* (Figure 6*I*). However, postnatal one-time feeding of S100A8 significantly increases the basal expression level of *Il10* (Figure 6*E*) and enhances the responsiveness of all LPS-inducible genes, that is, *Tnf*, *Il1b* and *Il10* (Figure 6*J*). Cross-fostering experiments (Figure 6*K*–*N*) corroborated the importance of the enteral supply of S100-alarmins. Breast milk of WT mothers alone induces a full regulatory LPMP phenotype in *S100a9*$^{-/-}$ neonates with respect to CX3CR1 levels and *Tnf*, *Il10,* and *Tgfb1* expression and proper Treg expansion comparable to the co-fostered WT offspring. Instead, comparing WT neonates fostered by *S100a9*$^{-/-}$ mothers with co-fostered WT neonates reveals that sole endogenous production of S100A8-A9 leads only to a deficient expression of *Tnf* and *Tgfb1* and less strong Treg expansion. Collectively, these findings demonstrate that the perinatal enteral supply of S100A8 regulates the inflammatory responsiveness of LPMPs which promotes the postnatal development of Tregs in the gut.

High fS100A8-A9 During Infancy Prevents Dysbiosis-linked Diseases

NEC in preterm infants is preceded by gut dysbiosis with an early abundance of Enterobacteriaceae.[8,10] We determined the proportion of S100A8-expressing LPMPs in intestinal tissue samples obtained from NEC patients in comparison with age-matched controls (Supplementary Table 3). In NEC samples, barely any S100A8^{+} LPMPs are found compared with the high number of S100A8-expressing LPMPs in neonates without underlying intestinal inflammation (Figure 7*A*). The lack of enteral supply of S100A8-A9 due to the common practice of fasting in imminent NEC and the reduced endogenous production of S100A8-A9 in such patients suggest that S100-alarmins protect against NEC.

Another early-life disease associated with gut dysbiosis is neonatal LOS.[9,10] In the cohort of preterm infants, fS100A8-A9 levels preceding LOS are significantly lower than corresponding levels in infants without later sepsis (Figure 7*B*). fS100A8-A9 levels below 28 μg/g are associated with a 14-fold higher LOS risk than levels above 153 μg/g (Supplementary Table 6). In a murine model of *S aureus*–induced infection, we tested the prevention of neonatal sepsis by enterally supplied S100A8 (Figure 7*C*). One-time feeding of S100A8 at birth significantly lowers the death rate of *S100a9*$^{-/-}$ neonates from later sepsis (Figure 7*D*) along with an effective restriction of the cytokine response (Figure 7*E*) and bacterial burden (Figure 7*F*).

In the long term, gut dysbiosis has been identified as risk factor for the development of obesity.[7,41,42] We find comparable birth weights in WT and *S100a9*$^{-/-}$ pups, however, from day 10 on a significantly stronger weight gain in *S100a9*$^{-/-}$ mice compared with WT mice (Figure 7*G*). Fostering of *S100a9*$^{-/-}$ neonates by WT mothers significantly restricts the weight gain resulting in adult body weights comparable to that of co-fostered WT mice. In turn, WT mice that are fostered by *S100a9*$^{-/-}$ mothers end up with significantly higher body weights than the co-fostered WT offspring (Figure 7*H*). In humans, the body mass index (BMI) is a predictive value for early childhood obesity[43] and was monitored in our term infant birth cohort. The delta BMI from birth until 2 years of age was correlated with the mean of neonatal fS100A8-A9 levels while accounting for confounding influences. There is a strong inverse relationship; children with low fS100A8-A9 levels show a significantly stronger increase in their BMI over time compared with children with high fS100A8-A9 levels whose BMI at 2 years differs little from that at birth (Figure 7*I*).

Collectively, these data indicate a clinically highly relevant regulating impact of S100A8-A9 for the newborn's adaptation of intestinal immunity and suggest S100-alarmins as a valuable immunomodulatory measure for

Figure 7. Implications of neonatal intestinal S100-priming for health and disease. (*A*) *Left panels*, representative images of noninflammatory-diseased (control) and NEC-diseased human neonatal SI and LI tissue samples immunostained for S100A8 (*red*), CD68 (*green*), and nuclei (*blue*). *Right panels*, total number of CD68^{+} LPMPs (*blue dotted bar*), S100A8^{-}CD68^{+} LPMPs (*green bar*) and S100A8^{+}CD68^{+} LPMPs (*red bar*). Values represent mean counts in 4 high-power fields of n = 6 control SI, n = 5 NEC SI, n = 4 control LI, and n = 3 NEC LI. **P* <.05, ***P* <.005 (Mann-Whitney *U* test). (*B*) Mean of first-week fS100A8-A9 levels in preterm newborns without (n = 18) or with later occurrence of LOS (n = 17). Box plots show medians and interquartile ranges ± SD, **P* < .05 (likelihood ratio test of nested models with/without fS100A8-A9 as predictor of LOS, with gestational age included as covariate in both models). (*C*–*F*) *S100a9*$^{-/-}$ neonates fed after birth with S100A8 or phosphate-buffered saline (PBS) (Ctrl) followed by sepsis induction on day 3 by subcutaneous injection of *S aureus*. (*C*) Experimental setup. (*D*) Survival (Ctrl n = 8, S100A8 n = 9). ***P* < .005 (Mantel-Cox test). (*E*) Plasma cytokine levels (each group n = 7) and (*F*) bacterial burden (Ctrl n = 7, S100A8 n = 9) 24 hours after infection. *Bars* represent means ± SEM. CFU, colony-forming units. **P* < .05, ***P* < .01, ****P* < .005, *****P* < .001 (unpaired *t*-test). (*G*) Regression of body weights of male and female WT and *S100a9*$^{-/-}$ mice at indicated ages (each group n = 14–40 with equal sex distribution). *P* value determined per likelihood ratio test. (*H*) Body weight of adult (day 56) male WT and *S100a9*$^{-/-}$ mice co-fostered or cross-fostered during infancy (each group n = 10–17). **P* < .05, ***P* < .005, ****P* < .0001 (unpaired *t*-test). (*I*) Multivariable, confounder-adjusted linear regression depicting a significant inverse correlation between the mean of fS100A8-A9 from day 1 to 10 and the delta BMI from birth until 2 years of age in n = 72 human term infants. Best fit dotted regression line and *gray-shaded* SE. r, Pearson's correlation coefficient; *P* value of correlation.

the prevention of frequent dysbiosis-linked short- and long-term diseases.

Discussion

Our knowledge about what programming of neonatal immunity ensures optimal adaptation to the new extrauterine environment and what parameters determine such programming is fragmented. By detailed cellular and molecular studies in mice and 2 human birth cohorts we identified S100A8-A9 in the neonatal gut as a crucial host factor contributing to the successful co-development of gut mucosal immunity and the microbiota. We demonstrated that fS100A8-A9 levels are physiologically high in healthy term babies, particularly after VD compared with CS. Labor-induced stress is obviously the driving force for fS100A8-A9 release as levels after secondary CS (with preceding labor) are comparable to those after VD. We showed previously that breastfeeding provides infants with a large amount of S100A8-A923 and here identify LPMPs in the neonatal intestine as a second source of fS100A8-A9. The lower S100A8-A9 levels in breast milk of mothers that gave birth to a preterm infant,[23] slower increase of feeding volumes and higher CS rates are presumably the main reasons for reduced fS100A8-A9 in preterm compared with term babies. Other factors like birth weight, Apgar score, diet, and probiotics might also influence neonatal fS100A8-A9 and are currently analyzed in a prospective multicenter clinical study.

In our birth cohort, high fS100A8-A9 levels correlated with a specific gut microbiota state characterized by a strong expansion of Actinobacteria-like Bifidobacteriaceae and growth restriction of Gammaproteobacteria-like Enterobacteriaceae, implying an increase in health-beneficial gut metabolic activity including enriching short-chain fatty acid availability, although it is important to recognize this is a prediction from taxonomic composition which future studies must validate experimentally. Bifidobacteriaceae might contribute to the restriction of Enterobacteriaceae by producing acetate.[44] But for deeper species resolution and assessment of the gut functional potential future shotgun metagenomic analyses are essential. Enterobacteriaceae include important neonatal sepsis-causing opportunistic pathogens, eg, *E coli*, Enterobacter, and *Klebsiella* species.[9,10] *E coli* has even been proposed as marker of gut dysbiosis associated with diseases like NEC,[8,45] childhood atopy,[6] IBD,[46–48] and obesity.[49] In murine neonates, endogenously produced S100A8-A9 partly but enterally supplied S100A8-A9 via breast milk completely prevented the intestinal overgrowth of Enterobacteriaceae. Herein, S100A8-A9 likely acts in synergy with immunoregulatory human milk oligosaccharides, which prevent the mucosal attachment of pathobionts like *E coli*[50] while encouraging the growth of Bifidobacteriaceae.[51]

Our study demonstrates that S100A8-A9 in the intestine has obviously a dual role of extended relevance for the development of mucosal immunity. Directly after birth, under noninflammatory conditions, the exposure to S100A8-A9 induced microbial tolerance in LPMPs by restricting their LPS responsiveness in terms of *Tnf* and *Il1b* expression (eg, against the first wave of microbial colonization). This is similar to the S100A8-A9–mediated stress tolerization of newborn monocytes found previously.[17–19] After the neonatal period (in mice at >3 days), the amplifier function of S100A8-A9[19,34–36] applied by supporting the proinflammatory response of LPMPs (eg, in response to expanding microbiota and for defending possible pathogens). Particularly, however, S100A8-A9 consistently induced a regulatory LPMP phenotype with full effect of high CX3CR1 levels, and *Il10* and *Tgfb1* expression especially when supplied enterally, which promoted the expansion of Tregs. Our ex vivo as well as in vivo findings point to IL-10 playing a crucial role for the S100-mediated regulation of Tregs by LPMPs. The microbiome-shaping effect might amplify the expansion of Tregs by increasing the levels of commensal-derived butyrate.[52] Potential direct Treg-inducing activity of S100A8-A9 appears less relevant as its extracellular half-life is only approximately 24 hours,[35,53] whereas the Treg-promoting effect of a single feeding of S100A8 at birth was not evident before day 10. This is the first evidence that next to microbes also endogenous TLR-ligands like S100A8-A9 have crucial instructing function for the newborn intestinal immune system. The here-identified immunomodulatory effects of fS100A8-A9 explain well the resulting shaping effect on the microbiota composition. CX3CR1, IL-10, and TGF-β as well as Tregs have been demonstrated to be important factors controlling the gut microbiota composition, specifically also the expansion of Enterobacteriaceae.[54–57] Interestingly, signs of colitis in IL10R-deficient mice are absent during the first 2 weeks of life, while intestinal inflammation and macrophage dysfunction begin during the third week, concomitant with weaning.[58] Thus, the immunoregulatory effects other than IL-10 induction might be of particular relevance for the S100-mediated impact on the gut microbial ecology.

The clinical relevance of S100-programming of neonatal gut immunity is shown for NEC and LOS, frequent dysbiosis-associated diseases in preterm infants. We observed virtually no expression of S100A8-A9 in the intestine of patients with NEC. This finding is supported by a previous observation of unusually low fS100A8-A9 concentrations in the meconium of patients with later NEC.[59] In contrast, due to the physiologically increased basal levels in neonates, which moreover are developmentally controlled (GA and age)[59,60] with high interindividual variation,[61] fS100A8-A9 is no valuable biomarker in NEC like in IBD of older children and adults.[22] In our cohort, low fS100A8-A9 levels reliably predicted a high LOS risk even when controlling for GA. Experimentally, 1-time feeding of S100A8 to *S100a9*$^{-/-}$ neonates prevented fatal outcomes of later sepsis. It might appear contradictory that there was only one *E coli*–positive LOS case within the blood-culture positive subjects of our preterm infant cohort while Enterobacteriaceae expand at low fS100A8-A9 levels. On the other side, our study might suggest a new perspective on the linkage between gut dysbiosis and sepsis by suggesting both being separate consequences of insufficiently S100-primed neonatal

immunity that predisposes to unregulated immune responses to microbial challenges.[17–19]

The here-identified link between low neonatal fS100A8-A9 levels and a disproportionate weight gain during childhood points to a role in dysbiosis-associated long-term diseases. Skewed gut microbiota composition has been shown to predispose to the development of obesity.[7,41,42,49] In the mouse model, 1-time feeding of S100A8 after birth prevented excessive weight gain in adolescent *S100a9*$^{-/-}$ mice. Future clinical studies in humans will have to clarify whether food supplement with S100A8-A9 during infancy prevents the development of unfavorable gut microbiota signatures and therewith associated diseases to promote long-term health.

Collectively, our data demonstrate for the first time that abundant fS100A8-A9 trains intestinal mucosal immunity by regulating the inflammatory programming and cellular development during infancy, which goes along with colonization by a favorable microbiota. Intestinal S100A8-A9 deficiency increases the risk of newborn individuals to develop unfavorable gut microbiota signatures and associated diseases. Animal data suggest nutritional supplementation of S100-alarmins to high-risk neonates as promising preventive measure.

Supplementary Material

Note: To access the supplementary material accompanying this article, visit the online version of *Gastroenterology* at www.gastrojournal.org, and at https://doi.org/10.1053/j.gastro.2020.08.019.

References

1. Macpherson AJ, Agüero MG de, Ganal-Vonarburg SC. How nutrition and the maternal microbiota shape the neonatal immune system. Nat Rev Immunol 2017; 17:508–517.
2. Gensollen T, Iyer SS, Kasper DL, et al. How colonization by microbiota in early life shapes the immune system. Science 2016;352:539–544.
3. Belkaid Y, Harrison OJ. Homeostatic Immunity and the Microbiota. Immunity 2017;46:562–576.
4. **Forslund K, Hildebrand F, Nielsen T, Falony G, Le Chatelier E**, et al. Disentangling type 2 diabetes and metformin treatment signatures in the human gut microbiota. Nature 2015;528:262–266.
5. Kamada N, Seo S-U, Chen GY, et al. Role of the gut microbiota in immunity and inflammatory disease. Nat Rev Immunol 2013;13:321–335.
6. Penders J, Thijs C, van den Brandt, Piet A, et al. Gut microbiota composition and development of atopic manifestations in infancy: the KOALA Birth Cohort Study. Gut 2007;56:661–667.
7. Turnbaugh PJ, Hamady M, Yatsunenko T, et al. A core gut microbiome in obese and lean twins. Nature 2009; 457:480–484.
8. Warner BB, Deych E, Zhou Y, et al. Gut bacteria dysbiosis and necrotising enterocolitis in very low birthweight infants: a prospective case-control study. Lancet 2016;387:1928–1936.
9. Carl MA, Ndao IM, Springman AC, et al. Sepsis from the gut: the enteric habitat of bacteria that cause late-onset neonatal bloodstream infections. Clin Infect Dis 2014; 58:1211–1218.
10. **Graspeuntner S, Waschina S**, Künzel S, et al. Gut dysbiosis with Bacilli dominance and accumulation of fermentation products precedes late-onset sepsis in preterm infants. Clin Infect Dis 2018.
11. **Gregory KE, Samuel BS**, Houghteling P, et al. Influence of maternal breast milk ingestion on acquisition of the intestinal microbiome in preterm infants. Microbiome 2016;4:68.
12. Grönlund MM, Lehtonen OP, Eerola E, et al. Fecal microflora in healthy infants born by different methods of delivery: permanent changes in intestinal flora after cesarean delivery. J Pediatr Gastroenterol Nutr 1999; 28:19–25.
13. Schwartz S, Friedberg I, Ivanov IV, et al. A metagenomic study of diet-dependent interaction between gut microbiota and host in infants reveals differences in immune response. Genome Biol 2012;13:r32.
14. Arboleya S, Solís G, Fernández N, et al. Facultative to strict anaerobes ratio in the preterm infant microbiota: a target for intervention? Gut microbes 2012;3:583–588.
15. Baumann-Dudenhoeffer AM, D'Souza AW, Tarr PI, et al. Infant diet and maternal gestational weight gain predict early metabolic maturation of gut microbiomes. Nat Med 2018;24:1822–1829.
16. **Dominguez-Bello MG, Costello EK**, Contreras M, et al. Delivery mode shapes the acquisition and structure of the initial microbiota across multiple body habitats in newborns. Proc Natl Acad Sci U S A 2010;107:11971–11975.
17. **Ulas T, Pirr S**, Fehlhaber B, et al. S100-alarmin-induced innate immune programming protects newborn infants from sepsis. Nat Immunol 2017;18:622–632.
18. Heinemann AS, Pirr S, Fehlhaber B, et al. In neonates S100A8/S100A9 alarmins prevent the expansion of a specific inflammatory monocyte population promoting septic shock. FASEB J 2017;31:1153–1164.
19. **Austermann J, Friesenhagen J**, Fassl SK, et al. Alarmins MRP8 and MRP14 induce stress tolerance in phagocytes under sterile inflammatory conditions. Cell Rep 2014;9:2112–2123.
20. **Vogl T, Stratis A**, Wixler V, et al. Autoinhibitory regulation of S100A8/S100A9 alarmin activity locally restricts sterile inflammation. J Clin Invest 2018;128:1852–1866.
21. Vogl T, Leukert N, Barczyk K, et al. Biophysical characterization of S100A8 and S100A9 in the absence and presence of bivalent cations. Biochim Biophys Acta 2006;1763:1298–1306.
22. Foell D, Wittkowski H, Roth J. Monitoring disease activity by stool analyses: from occult blood to molecular markers of intestinal inflammation and damage. Gut 2009;58:859–868.
23. **Pirr S, Richter M**, Fehlhaber B, et al. High Amounts of S100-Alarmins Confer Antimicrobial Activity on Human Breast Milk Targeting Pathogens Relevant in Neonatal Sepsis. Front Immunol 2017;8:1822.

24. Savino F, Castagno E, Calabrese R, et al. High faecal calprotectin levels in healthy, 64 exclusively breast-fed infants. Neonatology 2010;97:299–304.
25. Guilliams M, Scott CL. Does niche competition determine the origin of tissue-resident macrophages? Nat Rev Immunol 2017;17:451–460.
26. Ginhoux F, Guilliams M. Tissue-Resident Macrophage Ontogeny and Homeostasis. Immunity 2016;44:439–449.
27. **Bain CC, Bravo-Blas A**, Scott CL, et al. Constant replenishment from circulating monocytes maintains the macrophage pool in the intestine of adult mice. Nat Immunol 2014;15:929–937.
28. Manitz M-P, Horst B, Seeliger S, et al. Loss of S100A9 (MRP14) results in reduced interleukin-8-induced CD11b surface expression, a polarized microfilament system, and diminished responsiveness to chemoattractants in vitro. Mol Cell Biol 2003;23:1034–1043.
29. **Hobbs JAR, May R, Tanousis K**, et al. Myeloid cell function in MRP-14 (S100A9) null mice. Mol Cell Biol 2003;23:2564–2576.
30. Graspeuntner S, Bohlmann MK, Gillmann K, et al. Microbiota-based analysis reveals specific bacterial traits and a novel strategy for the diagnosis of infectious infertility. PloS One 2018;13:e0191047.
31. Corbin BD, Seeley EH, Raab A, et al. Metal chelation and inhibition of bacterial growth in tissue abscesses. Science 2008;319:962–965.
32. Achouiti A, Vogl T, Urban CF, et al. Myeloid-related protein-14 contributes to protective immunity in gram-negative pneumonia derived sepsis. PLoS Pathog 2012;8:e1002987.
33. **Damo SM, Kehl-Fie TE**, Sugitani N, et al. Molecular basis for manganese sequestration by calprotectin and roles in the innate immune response to invading bacterial pathogens. Proc Natl Acad Sci U S A 2013;110:3841–3846.
34. Vogl T, Tenbrock K, Ludwig S, et al. MRP8 and MRP14 are endogenous activators of Toll-like receptor 4, promoting lethal, endotoxin-induced shock. Nat Med 2007;13:1042–1049.
35. Viemann D, Strey A, Janning A, et al. Myeloid-related proteins 8 and 14 induce a specific inflammatory response in human microvascular endothelial cells. Blood 2005;105:2955–2962.
36. Frosch M, Vogl T, Seeliger S, et al. Expression of myeloid-related proteins 8 and 14 in systemic-onset juvenile rheumatoid arthritis. Arthritis Rheum 2003;48:2622–2626.
37. Murai M, Turovskaya O, Kim G, et al. Interleukin 10 acts on regulatory T cells to maintain expression of the transcription factor Foxp3 and suppressive function in mice with colitis. Nat Immunol 2009;10:1178–1184.
38. Hadis U, Wahl B, Schulz O, et al. Intestinal Tolerance Requires Gut Homing and Expansion of FoxP3+ Regulatory T Cells in the Lamina Propria. Immunity 2011;34:237–246.
39. Chen W, Jin W, Hardegen N, et al. Conversion of peripheral CD4+CD25- naive T cells to CD4+CD25+ regulatory T cells by TGF-beta induction of transcription factor Foxp3. The J Exp Med 2003;198:1875–1886.
40. Denning TL, Wang Y-cC, Patel SR, et al. Lamina propria macrophages and dendritic cells differentially induce regulatory and interleukin 17-producing T cell responses. Nat Immunol 2007;8:1086–1094.
41. **Le Chatelier E, Nielsen T, Qin J, Prifti E**, et al. Richness of human gut microbiome correlates with metabolic markers. Nature 2013;500:541–546.
42. Ley RE, Turnbaugh PJ, Klein S, et al. Microbial ecology: human gut microbes associated with obesity. Nature 2006;444:1022–1023.
43. Roy SM, Spivack JG, Faith MS, et al. Infant BMI or Weight-for-Length and Obesity Risk in Early Childhood. Pediatrics 2016;137.
44. Fukuda S, Toh H, Hase K, et al. Bifidobacteria can protect from enteropathogenic infection through production of acetate. Nature 2011;469:543–547.
45. **Ward DV, Scholz M**, Zolfo M, et al. Metagenomic Sequencing with Strain-Level Resolution Implicates Uropathogenic E. coli in Necrotizing Enterocolitis and Mortality in Preterm Infants. Cell Rep 2016;14:2912–2924.
46. Palmela C, Chevarin C, Xu Z, et al. Adherent-invasive Escherichia coli in inflammatory bowel disease. Gut 2018;67:574–587.
47. Fang X, Monk JM, Mih N, et al. Escherichia coli B2 strains prevalent in inflammatory bowel disease patients have distinct metabolic capabilities that enable colonization of intestinal mucosa. BMC Syst Biol 2018;12:66.
48. Kittana H, Gomes-Neto JC, Heck K, et al. Commensal Escherichia coli Strains Can Promote Intestinal Inflammation via Differential Interleukin-6 Production. Front Immunol 2018;9:2318.
49. **Gao R, Zhu C, Li H**, et al. Dysbiosis Signatures of Gut Microbiota Along the Sequence from Healthy, Young Patients to Those with Overweight and Obesity. Obesity 2018;26:351–361.
50. Manthey CF, Autran CA, Eckmann L, et al. Human milk oligosaccharides protect against enteropathogenic Escherichia coli attachment in vitro and EPEC colonization in suckling mice. J Pediatr Gastroenterol Nutr 2014;58:165–168.
51. Underwood MA, Davis JCC, Kalanetra KM, et al. Digestion of Human Milk Oligosaccharides by Bifidobacterium breve in the Premature Infant. J Pediatr Gastroenterol Nutr 2017;65:449–455.
52. **Furusawa Y, Obata Y, Fukuda S**, et al. Commensal microbe-derived butyrate induces the differentiation of colonic regulatory T cells. Nature 2013;504:446–450.
53. Hirono K, Foell D, Xing Y, et al. Expression of myeloid-related protein-8 and -14 in patients with acute Kawasaki disease. J Am Coll Cardiol 2006;48:1257–1264.
54. Kim Y-I, Song J-H, Ko H-J, et al. CX3CR1(+) Macrophages and CD8(+) T Cells Control Intestinal IgA Production. J Immunol 2018;201:1287–1294.
55. Zhong Y, Cantwell A, Dube PH. Transforming growth factor beta and CD25 are important for controlling systemic dissemination following Yersinia enterocolitica infection of the gut. Infect Immun 2010;78:3716–3725.
56. Duque-Correa MA, Karp NA, McCarthy C, et al. Exclusive dependence of IL-10Ralpha signalling on intestinal

microbiota homeostasis and control of whipworm infection. PLoS Pathog 2019;15:e1007265.
57. **Maharshak N, Packey CD**, Ellermann M, et al. Altered enteric microbiota ecology in interleukin 10-deficient mice during development and progression of intestinal inflammation. Gut Microbes 2013;4:316–324.
58. Redhu NS, Bakthavatchalu V, Conaway EA, et al. Macrophage dysfunction initiates colitis during weaning of infant mice lacking the interleukin-10 receptor. Elife 2017;6.
59. Zoppelli L, Guttel C, Bittrich H-J, et al. Fecal calprotectin concentrations in premature infants have a lower limit and show postnatal and gestational age dependence. Neonatology 2012;102:68–74.
60. Lee YM, Min C-Y, Choi YJ, et al. Delivery and feeding mode affects fecal calprotectin levels in infants <7months old. Early Hum Dev 2017;108:45–48.
61. van Zoonen, Anne GJF, Hulzebos CV, Muller Kobold AC, et al. Serial fecal calprotectin in the prediction of necrotizing enterocolitis in preterm neonates. J Pediatr Surg 2019;54:455–459.

Author names in bold designate shared co-first authorship.

Received February 7, 2020. Accepted August 9, 2020.

Correspondence
Address correspondence to Dorothee Viemann, PhD, MD, Department of Pediatric Pneumology, Allergy and Neonatology, Hannover Medical School, Carl-Neuberg-Straße 1, 30625 Hannover, Germany. e-mail: Viemann.Dorothee@mh-hannover.de.

Acknowledgments
We thank Christiane Ritter for technical assistance and Yvonne Lueder for advice on image analysis. We acknowledge the assistance of the Cell Sorting Core Facility of the Hannover Medical School supported in part by Braukmann-Wittenberg-Herz-Foundation and the German Research Foundation. We are grateful to all parents contributing to this study.

CRediT Authorship Contributions
Maike Willers, PhD (Conceptualization: Equal; Data curation: Lead; Formal analysis:
Equal; Investigation: Lead; Methodology: Lead; Writing – original draft: Lead)
Thomas Ulas, PhD (Data curation: Lead; Formal analysis: Lead; Software: Equal;
Writing – original draft: Equal). Lena Völlger, PhD (Data curation: Equal; Formal analysis: Equal; Investigation: Lead; Methodology: Lead; Supervision: Supporting; Writing – original draft: Supporting). Thomas Vogl, PhD (Funding acquisition: Supporting; Investigation: Supporting; Methodology: Supporting; Validation: Supporting; Writing – original draft: Supporting). Anna S. Heinemann, N/A (Conceptualization: Supporting; Data curation: Supporting; Investigation: Supporting; Methodology: Supporting). Sabine Pirr, MD (Conceptualization: Equal; Funding acquisition: Supporting; Investigation: Equal; Project administration: Supporting; Supervision: Equal; Writing – original draft: Supporting). Julia Pagel, MD (Data curation: Supporting; Investigation: Supporting). Beate Fehlhaber, PhD (Data curation: Supporting; Formal analysis: Supporting; Investigation: Supporting; Methodology: Supporting). Olga Halle, Ph.D. (Conceptualization: Supporting; Formal analysis: Equal; Investigation: Supporting; Methodology: Lead). Jennifer Schöning, N/A (Formal analysis: Equal; Methodology: Equal; Supervision: Supporting; Visualization: Lead). Sabine Schreek, N/A (Formal analysis: Equal; Investigation: Equal; Methodology: Equal). Ulrike Löber, PhD (Formal analysis: Supporting). Morgan Essex, PhD (Formal analysis: Supporting). Peter Hombach, N/A (Data curation: Supporting; Formal analysis: Supporting;
Methodology: Supporting; Software: Supporting). Simon Graspeuntner, PhD (Data curation: Supporting; Formal analysis: Supporting; Software: Supporting). Marijana Basic, PhD (Investigation: Supporting; Methodology: Supporting). Andre Bleich, PhD (Methodology: Supporting; Resources: Supporting). Katja Cloppenborg-Schmidt, N/A (Data curation: Supporting; Formal analysis: Supporting; Investigation: Supporting; Methodology: Equal).
Sven Künzel, PhD (Data curation: Equal; Methodology: Equal). Danny Jonigk, MD (Data curation: Supporting; Investigation: Supporting; Methodology: Supporting). Jan Rupp, MD, PhD (Resources: Supporting; Supervision: Supporting). Gesine Hansen, MD, PhD (Resources: Supporting). Reinhold Förster, PhD (Resources: Supporting). John F. Baines, PhD (Conceptualization: Supporting; Methodology: Supporting; Resources: Supporting). Christoph Härtel, MD, PhD (Data curation: Supporting; Formal analysis: Supporting;
Writing – review & editing: Supporting). Joachim L. Schultze, PhD, MD (Resources: Supporting). Sofia K. Forslund, PhD (Formal analysis: Lead; Methodology: Supporting;
Supervision: Supporting; Validation: Lead; Writing – review & editing: Equal). Johannes Roth, MD, PhD (Conceptualization: Supporting; Data curation: Supporting; Formal analysis: Supporting; Funding acquisition: Supporting; Resources: Supporting; Writing – review & editing: Supporting). Dorothee Viemann, PhD, MD (Conceptualization: Lead; Funding acquisition: Lead; Investigation: Equal; Project administration: Lead; Supervision: Lead; Writing – review & editing: Lead).

Conflict of interest
The authors disclose no conflicts.

Funding
This work was supported by grants to Dorothee Viemann from the Volkswagen Foundation (Az 90 005), the Appenrodt Foundation and the Deutsche Forschungsgemeinschaft (DFG) (VI 538/6-1), grants by the DFG to Johannes Roth and Thomas Vogl (CRC1009, B08 and B09) and to Dorothee Viemann, Gesine Hansen, and Reinhold Förster by the DFG under Germany`s Excellence Strategy – EXC 2155 'RESIST' – Project ID 39087428. John F. Baines was funded by the DFG under Germany`s Excellence Strategy – EXC 22167-390884018 and CRC1182. Christoph Härtel was funded by the Federal Ministry of Education and Research (BMBF; PRIMAL clinical study, No. 01GL1746A), the University of Lübeck and the Lübeck-Hilfe für krebskranke Kinder e.V. Joachim L. Schultze is a member of the Excellence Cluster ImmunoSensation.

Supplementary Experimental Procedures

Study Population

Stool samples (n = 517) were collected from 2 birth cohorts of healthy term and preterm infants. Term infants (n = 72, Supplementary Table 1) were prospectively enrolled at the Hannover Medical School from May 2015 to June 2017. The inclusion criteria were being born healthy and appropriate for gestational age (GA) with a GA of 37 0/7 to 41 6/7 weeks, an Apgar score of ≥8 after 5 minutes, and intended breast feeding as predominant diet. GA was calculated on the basis of the mother's last menstrual period. When early ultrasound at 11 to 13 6/7 weeks of gestation using fetal crown–rump length deviated by more than 7 days, dating was done by ultrasound. After written informed consent was obtained from parents, d1 and d2 stool samples were collected by medical staff from diapers and after that by parents on d10, d30, and d90 and at 6 and 12 months. Infants from pregnancies that involved in vitro fertilization, multiple gestations, births that resulted from maternal trauma, and newborns with any congenital malformations or chromosomal anomalies, with clinical or laboratory signs of amnion infection syndrome or if the mother or infant received any peripartal antibiotic therapy were excluded. Cohort subjects were followed until 2.5 years of age. Metadata collected on maternal characteristics were age and BMI at delivery and prepregnancy BMI. Child-related data included the BMI (birth, d30, 3m, 6m, 1y, and 2y), diet (exclusive breastfeeding, mixed feeding with formula, age at introduction of solid food) history of allergies, infections, antibiotics and inhalations during the first year of life. Information on life circumstances included the presence of siblings, smoking status of the parents, pets, and residence (county/urban).

The birth cohort of preterm infants was established between January 2012 and January 2017 and included 49 preterm infants born at a GA of 23 0/7 to 31 6/7 weeks in the Neonatal Intensive Care Unit of the Department of Pediatrics at the University of Lübeck (Supplementary Table 2). Infants with lethal malformations or congenital anomalies of the gastrointestinal tract were excluded. LOS was defined as sepsis starting after 72 hours of life. LOS was diagnosed with the occurrence of ≥2 clinical signs of systemic inflammatory response and 1 laboratory sign. Clinical signs of LOS included temperature >38°C or <36.5°C, tachycardia >200/min, new onset or increased frequency of bradycardias or apneas, hyperglycemia >140 mg/dL, base excess <−10 mval/L, changed skin color, and increased oxygen need. Laboratory signs of LOS were C-reactive protein >10 mg/L, platelet count <100/nL, immature/total neutrophil ratio >0.2, and white blood cell count <5/nL. Blood culture confirmed LOS was defined as clinical LOS with bacterial growth in the blood culture, which was taken before commencing antibiotic therapy. LOS occurred in n = 22 cases at a mean age of 14.8 days ± 4.9, from which 11 were blood culture proven (*Staphylococcus haemolyticus* 5, *Staphylococcus. epidermidis* 4, *Escherichia coli* 1, *Enterococcus faecalis* 1). Fecal samples were collected from the preterm birth cohort on days 1 to 7, 8 to 12, 13 to 19, and 20 to 30 by medical staff from diapers or after rectal enema with 37°C NaCl 0.9% solution. Stool was immediately stored at −20°C, and transferred to −80°C within 3 days.

Human intestinal tissue samples were obtained upon written informed consent from n = 8 adult patients and n = 18 newborn infants and included SI and LI resections (Supplementary Table 3). Biopsies in adults were performed due to the exclusion of malignancies or IBD or in the context of ileostomy or bile duct carcinoma and served as adult controls. Intestinal tissue from newborn infants was resected due to the diagnosis of NEC (n = 8) or in the context of inborn atresia, perforation, stenosis, volvulus, or ileostomy (n = 10). Biopsies of the latter served as neonatal intestinal controls. The tissue was formalin-fixed and paraffin-embedded and used for immunofluorescence microscopy.

Ethics Statement

Protocols and usage of human biomaterial were approved by the Institutional Review Board of the Hannover Medical School (no. 6031-2015 and 3381-2016) and University of Lübeck (no. AZ15-304). Written informed consent was obtained from parents or legal representatives on behalf of the infants enrolled in our study. Mouse experiments were carried out in accordance with German Animal Welfare Legislation and performed as approved by the Lower Saxony State Office for Consumer and Food Safety, Germany (approval no. 33.9-42502-04-15/1951 and 33.12-42502-04-15/1969).

Reagents and Bacteria

LPS (*E coli* 055:B5) was purchased from Sigma (Taufkirchen, Germany). Murine S100A8 was recombinantly expressed in *E coli* BL21(DE3) and purified as described earlier.[1]Klicken oder tippen Sie hier, um Text einzugeben. *S aureus* strain Newman, GenBank accession number AP009351.1, was used and inoculated 1:100 in Todd-Hewitt-Bouillon (Roth, Karlsruhe, Germany) and incubated at 37°C until late-logarithmic phase was reached (OD_{600} = 0.7–0.8). Suspensions were adjusted to a concentration of 1×10^{10}/mL and stored at −80°C. Infection dose was controlled by serial dilutions and plating blood-agar (Oxoid, Wesel, Germany) for colony-counting.

Fecal S100A8-A9 (fS100A8-A9)

Fecal sample aliquots were suspended in extraction buffer adopted from Hycult Biotech's H325 Human Calprotectin enzyme-linked immunosorbent assay (ELISA) kit. Suspensions were thoroughly vortexed, filtered through a 100-μm cell strainer, and then incubated on a shaker on ice for 20 minutes. The homogenates were centrifuged for 20 minutes at 10,000*g* at 4°C. The upper portion of the supernatants was pipetted off, frozen, and stored at −80°C

until quantification of fS100A8-A9 by an in-house ELISA as described previously.[1,2]

Immunofluorescence Microscopy

Human paraffin-embedded intestinal tissues sections were deparaffinized in Roti-Histol (Roth), rehydrated and subjected to heat-induced antigen retrieval in citrate buffer. In NEC samples, resection margins unaffected from necrosis and severe inflammation were analyzed. Before antibody staining, the tissue was washed and blocked with 5% skim milk powder in tris-buffered saline (TBS) to minimize nonspecific binding. The slides were stained overnight at 4°C in the dark with mouse anti-human CD68 monoclonal antibody (mAb) (M0814, Dako, Hamburg, Germany) and rabbit anti-human S100A8 polyclonal antibody (purified by T.V.) followed by AlexaFluor488 donkey anti-mouse and AlexaFluor555 donkey anti-rabbit secondary antibodies (both Life Technologies, Darmstadt, Germany). Tissue was mounted in VECTASHIELD Antifade Mounting Medium with 4′,6-diamidino-2-phenylindole (DAPI) (Vector Laboratories, Burlingame, CA). Images were acquired using the Zeiss Axioplan 2 fluorescence microscope with a Zeiss EC Plan-Neofluar 10x/0.3 objective and a Zeiss EC Plan-Neofluar 40x/0.75 Ph2 objective, the AxioCam Color camera and AxioVision 40 v4.8.2 imaging software from Zeiss (Jena, Germany). The number of $CD68^+$ and $S100A8^+$ cells in human intestinal tissues sections was determined per high-power field by manual counting performed by 2 blinded observers.

Murine colon tissue was embedded in Tissue-Tek O.C.T. Compound (Sakura Finetek, Torrance, CA) without prior fixation, frozen on dry ice, and stored at −80°C. Cryosections (8 μm) were fixed with acetone and stored at −20°C. Sections were rehydrated in TBS supplemented with 0.1% Tween20 (TBST) and blocked with 5% rat serum. For immunostaining, the following antibodies were used: rat anti-mouse forkhead box P3 (FoxP3) mAb (FJK-16s, eBioscience, San Diego, CA), rat anti-mouse CD3 mAb (17A2, purified in the Förster laboratory, Hannover, Germany), rat anti-mouse CD4 mAb (GK1.5, purified in the Förster laboratory), rat anti-mouse F4/80 mAb (BM8; Biolegend, San Diego, CA), and mouse anti-mouse Cx3cr1 mAb (SA011F11, BioLegend). Images were acquired using an Olympus BX61 epifluorescence microscope. For the analysis of Cx3cr1 expression on $F4/80^+$ LPMPs, at least 5 randomly selected images acquired from proximal, mid and distal LI sections prepared from 2 WT and 2 $S100a9^{-/-}$ neonatal mice (day 10) were analyzed per condition. The same exposure times were used for the acquisition of the read-out channel for Cx3r1 staining. The intensity of Cx3cr1 expression was measured by defining regions of interest (ROIs) encompassing F4/80-stained areas and measuring the maximum fluorescence intensity of the Cx3cr1 signal in ROIs. For the analysis of Tregs, $CD3^+CD4^+$ T cells with a FoxP3-positive nucleus were counted manually by 2 blinded observers.

Mice and Mouse Studies

The following mouse strains used in this study were housed under specific pathogen-free conditions at the Central Animal Facility at Hannover Medical School. The Foxp3-eGFP reporter mouse B6.Cg-Foxp3 tm1 Mal/J was obtained from Jackson Laboratory (Bar Harbor, ME) and used for the isolation of naïve $CD4^+$ T cells from adult spleens. C57BL/6J WT mice purchased from Charles River (Sulzfeld, Germany) and $S100a9^{-/-}$ mice (C57BL/6 background)[3] were constantly bred and litters used randomly at indicated ages to harvest colon contents, LIs, mesenteric lymph nodes (mLN), and celiac lymph nodes (cLN). No animals needed to be excluded from the studies. WT and $S100a9^{-/-}$ mothers were co-housed for at least a week before and after mating until day 18 of pregnancy and then separated for delivery. In indicated experiments, $S100a9^{-/-}$ pups were supplemented within 24 hours after birth either by IP injection of 2.5 μg S100A8 in 20 μL phosphate-buffered saline (PBS) or enteral feeding of 5 μg S100A8 in 20 μL PBS. Mice supplemented with PBS alone served as controls. For cross-fostering experiments, mating of WT and $S100a9^{-/-}$ mice was terminated to exchange litters within 12 hours after birth.

Isolation of LPMPs From the Murine Colon

LPMPs were isolated from harvested murine LIs using a modified protocol published elsewhere.[4] After dissection, the colon was opened longitudinally, the stool was collected and the tissue was thoroughly washed in ice-cold PBS. In day 3 and day 10 neonates, 3 to 4 LIs were pooled for one experiment. To remove intestinal epithelial cells, the tissue was cut into 0.5-cm pieces and incubated in prewarmed PBS supplemented with 2 mM EDTA for 15 minutes at 37°C with agitation. Subsequently, the tissue was repeatedly shaken, minced, and digested for up to 60 minutes at 37°C under constant agitation in RPMI medium (Lonza, Basel, Switzerland) containing 10% fetal calf serum (FCS), 1% penicillin/streptomycin, 75 μg/mL liberase, and 30 U DNase I (both Sigma). The digested tissue was filtered through a 100-μm cell strainer followed by a 70-μm cell strainer. Thereby isolated lamina propria mononuclear cells (LPMCs) were pelleted and resuspended in PBS containing 2 mM EDTA and 2% bovine serum albumin (FACS buffer) and used for cell number determination, flow cytometry studies and cell sorting. LPMPs were sorted at the central Research Facility Cell Sorting at the Hannover Medical School, either on FACSAria Fusion and FACSAria IIu (both BD Biosciences, Heidelberg, Germany) or on MoFlo XDP (Beckmann-Coulter, Krefeld, Germany). Therefore, LPMPs were stained as described below and sorted by gating on live $CD45^+CD11b^+F4/80^{+/\text{interm}}$ cells. The purity of isolated LPMPs was >90%. For the preparation of cytospins, LPMPs were seeded on superfrost slides and centrifuged at 300*g* for 5 minutes. Cells were fixed in 2% paraformaldehyde (PFA) and stained with hematoxylin/eosin. Remaining LPMPs were used for gene expression studies and ex vivo stimulation assays.

Flow Cytometry

All staining panels included a Fixable Viability Dye eFluor 506 (eBioscience) to exclude dead cells as well as CD16/CD32 (2.4G2, BioLegend) for blocking purposes. Staining was performed for 30 minutes in the dark at 4°C. After staining cells were fixed with 2% PFA.

LPMPs

For the analysis of F4/80^{hi}CD11b$^{+/-}$Ly6G^{-}CD11c^{-} YS-LPMPs and F4/80^{+}CD11b^{+}Ly6G^{-}CD11c^{-} BD-LPMPs, colonic LPMC single-cell suspensions were stained with rat anti-mouse CD45 mAb (30F-11), rat anti-mouse F4/80 mAb (BM8), hamster anti-mouse CD11c mAb (N418), rat anti-mouse CD11b mAb (M1/70) (all eBioscience) and rat anti-mouse Ly6G mAb (1A8, BioLegend) and gated as illustrated in Supplementary Figure 4*A* and *B*.

Tregs

For the analysis of Tregs, single-cell suspensions of colonic LPMCs, mLNs and cLNs were first stained extracellularly using rat anti-mouse CD45 mAb (30-F11), hamster anti-mouse CD3e mAb (145-2C11) and rat anti-mouse CD4 mAb (RM 4-5) (all eBioscience). For intracellular staining, cells were fixed in 2% PFA for 30 min at room temperature. Subsequently, cells were stained with rat anti-mouse FoxP3 mAb (FJK-16s, eBioscience) in FACS buffer with 0.5% saponin and 0.2% Tween20 for another 30 min at 4°C in the dark. Gating was done as shown in Supplementary Figure 5*A*.

Data Acquisition and Analyses

All flow cytometry analyses were performed using a FACS Canto II flow cytometer (BD Biosciences). Data were analyzed using DIVA software v8.0.1 (BD Biosciences) and Kaluza software v2.1 (Beckman Coulter, Miami Lakes, USA).

Cell Culture Conditions

Sorted LPMPs were seeded at a concentration of 1×10^6 cells/mL in RPMI medium supplemented with 10% FCS, 1% L-glutamin and 1% penicillin/streptomycin. After overnight culture LPMPs were stimulated for 4 hours with 100 ng/mL LPS. Control cells were incubated with PBS, respectively. Subsequently, LPS-stimulated cells were harvested and processed for gene expression studies.

In order to analyze the Treg-inducing capacity of WT and *S100a9*$^{-/-}$ LPMPs, naïve CD4^{+} T cells were isolated from cell suspensions prepared from spleens of adult Foxp3-eGFP reporter mice by using the Naïve CD4^{+} T Cell Isolation Kit from Miltenyi Biotec (Bergisch Gladbach, Germany) according to the manufacturer's instructions. Naïve T cells were co-cultured with LPMPs at ratios of 10:1 or 5:1 with a total cell concentration of 1×10^6 cells/mL in plates coated with 10 μg/mL of hamster anti-mouse CD3e mAb (145-2C11, eBioscience) and in the presence of 2 μg/mL of hamster anti-mouse CD28 mAb (37.51, eBioscience) and 10 ng/mL of IL-2 (Biolegend) without and with addition of 5 ng/mL of recombinant TGF-β (R&D, Minneapolis, MN) and 20 ng/mL of recombinant IL-10 (PeproTech, Rocky Hill, NJ). Cells were harvested after 4 days, stained with hamster anti-mouse CD3e mAb (145-2C11), rat anti-mouse CD4 mAb (RM 4-5) and Fixable Viability Dye eFluor 506 (all eBioscience) and analyzed by flow cytometry to determine the proportion of GFP-expressing Foxp3^{+} Tregs of CD3^{+}CD4^{+} T cells.

Quantitative Real Time PCR (qRT-PCR)

Total RNA was isolated using the NucleoSpin RNA II kit or NucleoSpin RNA XS kit (both Macherey-Nagel, Düren, Germany) according to the manufacturer's instructions. Complementary DNA (cDNA) was synthesized from 40 ng of total RNA using the SuperScript VILO Master Mix (Invitrogen, Carlsbad, CA). qRT-PCR was done as described previously.[5] The murine primers used for qRT-PCRs were *Gapdh* (F, GGACACTGAGCAAGAGAGGC; R, TTATGGGGGTCTGGGATGGA), *Tnf* (F, GATCGGTCCCCAAAGGGATG; R, GTGGTTTGTGAGTGTGAGGGT), *Il1b* (F, TGTCTTGGCCGAGGACTAAGG; R, TGGGCTGGACTGTTTCTAATGC), *Il10* (F, GGGTTGCCAAGCCTTATCG; R, TCTCACCCAGGGAATTCAAATG), and *Tgfb1* (F, AGGAGACGGAATACAGGGCT; R, ATGTCATGGATGGTGCCCAG). Sample data are presented as the fold change (FC) in expression compared with the controls as determined by the comparative ΔCt method or relative to the housekeeper *Gapdh*.

Microbiological Analysis of Murine Fecal Samples

Colon and cecum content were collected and suspended at 1 mL PBS/g feces. Serial dilutions were plated on Luria/Bertani agar (Roth) and incubated overnight under aerobic conditions at 37°C and 10% CO_2 to determine the numbers of CFU/g feces. For the selective growth of Enterobacteriaceae, diluted samples were plated on MacConkey agar (AppliChem, Darmstadt, Germany). Presumptive identification of *E coli* was made based on its characteristic colony morphology on the MacConkey agar (dry, donut shaped, dark pink in color, and surrounded with dark pink area).

Bioinformatics of 16S rRNA Gene Sequencing Data

The raw fastq files were processed using mothur version 1.40.5.[6] After generation of contigs, sequences containing ambiguous bases and sequences longer than 500 base pairs were removed. With the primer sequences from the MiSeq sequencing experiment, a custom reference alignment was generated using the SILVA reference version 132.[7] Sequences containing more than 8 homo polymers were excluded and sequences of nonbacterial origin removed. Chimeras were detected by the VSEARCH algorithm[8] as implemented in mothur. Classification of sequences was performed using the Greengenes database gg_13_8_99.[9] Sequences were clustered into operational taxonomic units (OTUs) according to their taxonomic assignment. The analysis after pre-processing in mothur was performed in R (version 3.6.1), mainly relying on the phyloseq package.[10] Following mapping of 16S reads to OTUs and binning at taxonomic class and family levels, total mapped read

abundances were down sampled using the rarefaction toolkit (RTK)[11] at default settings to account for differences in sampling depth as well as to compute alpha diversity metrics. For metagenome inference amplicon sequences were filtered, quality controlled, and taxonomically assigned using the LotuS pipeline.[12] Default parameters for the small subunit ribosomal ribonucleic acid and the MiSeq platform were used, while SILVA, Greengenes and HITdb (v1.00)[13] were used incrementally for taxonomic classification. Resulting abundance tables were normalized using RTK to 95% of the minimal column sum. Metagenome functional content was inferred from the raw amplicon sequences and processed taxonomic abundances using the PICRUSt2 method (v2.3.0-b).[14] MetaCyc pathway abundances were generated using the default map files and functional databases.[15] For nested model comparisons taxon abundances and MetaCyc pathway abundances (rarefied reads) were modeled individually using mixed effect models (R lme4 package) with fS100A8-A9, MOD, and age in days as fixed effects, with child identity as a random effect so as to account for the longitudinal nature of the data. Restricted maximum likelihood (REML) approximations were disabled to ensure likelihood ratio tests for nested model comparisons are accurate. For each tested variable (fS100A8-A9, MOD, age) a model omitting this feature was constructed and the 2 models compared in a likelihood ratio test (R lmtest package). In addition, each tested variable was directly compared against each tested feature (using a Mann-Whitney *U* [MWU] test for MOD and a Spearman test for age, and fS100A8-A9), with nonparametric directional effect sizes calculated as Spearman rho or Cliff's delta (R orddom package). Features were considered to be strongly and significantly affected by each feature if Benjamini-Hochberg–corrected *P* values for both nested model and simple test fulfilled false discovery rate (FDR) <0.1, and if absolute effect size exceeded 0.2.

Statistical Analysis

Statistical tests applied for 16S rRNA gene sequencing data analysis are described previously. Group comparison of fS100A8-A9 levels and proportions of $S100A8^{+}$ LPMPs in human tissue samples was performed by applying the 2-tailed MWU test. Age dependency of fS100A8-A9 levels was evaluated by running a Kruskal-Wallis test including post hoc Dunn's multiple comparison test. To test for differences between WT and *S100a9*$^{-/-}$ mice in gene expression or in fraction of Tregs measured at different ages, a nested model test was further used building generalized linear models (R lme4 package) of measured data using a Gamma distribution error model and setting zero values to a pseudocount floor of 1-e-10. Models with age and genotype were contrasted to models containing age only to test for main effect of genotype. Models with age, genotype, and an interaction term between them were contrasted to models containing age and genotype only to test for interaction effect between age and genotype. Models were compared using the R lmtest package. To test for differences between control and supplemented mice in gene expression or in fraction of Tregs, a nested model test was further used building generalized linear models (R lme4 package) of measured data using a Gamma distribution error model and setting zero values to a pseudocount floor of 1-e-10. Models with age and genotype were contrasted to models containing age only to test for main effect of supplementation. Models with age, supplementation, and an interaction term between them were contrasted to models containing age and supplementation only to test for interaction effect between age and supplementation. Models were compared using the R lmtest package. To test for differences between WT and *S100a9*$^{-/-}$ mice in proportion of Tregs, a nested model test was further employed building generalized linear models (R lme4 package) of proportions of Treg to $CD3^{+}$ cells using a binomial error model. Models with age and genotype were contrasted to models containing age only to test for main effect of genotype. Models with age, genotype and an interaction term between them were contrasted to models containing age and genotype only to test for interaction effect between age and genotype. Models were compared using the R lmtest package. Comparisons in co-culture assays and cross-fostering settings were evaluated by two-tailed *t*-tests. The difference between genotypes resp. intervention groups in the proportion of Enterobacteriaceae-positive fecal samples was tested by using the sign test. The association between fS100A8-A9 levels and the occurrence of LOS was assessed by calculating odds ratios and their 95% confidence intervals and by using a nested model test building generalized linear models (R lme4 package) of measured data using a Gamma distribution error model and setting zero values to a pseudocount floor of 1-e-10. The model with fS100A8-A9 and GA was contrasted to a model containing GA only to test for main effect of fS100A8-A9. Kaplan-Meier survival curves were generated using the Mantel-Cox test. The fS100A8-A9 levels of human term and preterm infants delivered by VD and CS and the body weight of WT and *S100a9*$^{-/-}$ mice was modeled against the fixed factor time (age). Linear models were fitted using the lm function of the standard R-package stats. Likelihood ratio tests of the full model against the control model without the fixed effect of MOD respective genotype were performed to determine the *P*-value of the difference between the mouse strains regarding gain of weight over time. Bivariate linear regression was used to assess how the mean of fS100A8-A9 during the first 10 days of life relates to the delta of the BMI from birth until 2 years of age of the children of the birth cohort of term human infants (Supplementary Table 1). We obtained crude and multivariable-adjusted estimates of this association. The multivariable-adjusted models included terms for maternal age and BMI at delivery, maternal prepregnancy BMI, birthweight (all continuous variables), offspring sex (boy or girl), diet (exclusive and mixed breastfeeding), antibiotics during the first year of life (yes/no), presence of siblings (yes/no), smoking status of the parents (yes/no), pets (yes/no), and residence (county/urban). P values $< .05$ were judged to be significant.

Supplementary References

1. Vogl T, Tenbrock K, Ludwig S, et al. Mrp8 and Mrp14 are endogenous activators of Toll-like receptor 4, promoting lethal, endotoxin-induced shock. Nat Med 2007; 13:1042–1049.
2. **Austermann J, Friesenhagen J**, Fassl SK, et al. Alarmins MRP8 and MRP14 induce stress tolerance in phagocytes under sterile inflammatory conditions. Cell Rep 2014;9:2112–2123.
3. Manitz M-P, Horst B, Seeliger S, et al. Loss of S100A9 (MRP14) results in reduced interleukin-8-induced CD11b surface expression, a polarized microfilament system, and diminished responsiveness to chemoattractants in vitro. Mol Cell Biol 2003;23:1034–1043.
4. Weigmann B, Tubbe I, Seidel D, et al. Isolation and subsequent analysis of murine lamina propria mononuclear cells from colonic tissue. Nat Protoc 2007; 2:2307–2311.
5. **Viemann D, Goebeler M**, Schmid S, et al. Transcriptional profiling of IKK2/NF-＼kappaB— and p38 MAP kinasedependent gene expression in TNF-＼alpha—stimulated primary human endothelial cells. Blood 2004;103:3365–3373.
6. Schloss PD, Westcott SL, Ryabin T, et al. Introducing mothur: open-source, platform-independent, community-supported software for describing and comparing microbial communities. Appl Environ Microbiol 2009;75:7537–7541.
7. **Pruesse E, Quast C**, Knittel K, et al. SILVA: a comprehensive online resource for quality checked and aligned ribosomal RNA sequence data compatible with ARB. Nucleic Acids Res 2007;35:7188–7196.
8. Rognes T, Flouri T, Nichols B, et al. VSEARCH: a versatile open source tool for metagenomics. PeerJ 2016;4:e2584.
9. DeSantis TZ, Hugenholtz P, Larsen N, et al. Greengenes, a chimera-checked 16S rRNA gene database and workbench compatible with ARB. Appl Environ Microbiol 2006;72:5069–5072.
10. McMurdie PJ, Holmes S. phyloseq: an R package for reproducible interactive analysis and graphics of microbiome census data. PLoS One 2013;8:e61217.
11. Saary P, Forslund K, Bork P, et al. RTK: efficient rarefaction analysis of large datasets. Bioinformatics 2017; 33:2594–2595.
12. Hildebrand F, Tadeo R, Voigt AY, et al. LotuS: an efficient and user-friendly OTU processing pipeline. Microbiome 2014;2:30.
13. Ritari J, Salojärvi J, Lahti L, et al. Improved taxonomic assignment of human intestinal 16S rRNA sequences by a dedicated reference database. BMC Genomics 2015;16:1056.
14. Douglas GM, Maffei VJ, Zaneveld J, et al. PICRUSt2: an improved and customizable approach for metagenome inference. bioRxiv preprint 2020, Available at: https://doi.org/10.1101/672295. Accessed May 1, 2020.
15. Caspi R, Billington R, Fulcher CA, et al. The MetaCyc database of metabolic pathways and enzymes. Nucleic Acids Res 2018;46:D633–D639.

Author names in bold designate shared co-first authorship.